1-1-2017

Statistical Shape and Intensity Modeling of the Shoulder

Irene Sintini
University of Denver

Statistical Shape and Intensity Modeling of the Shoulder

Abstract

Anatomical variability in the shoulder is inherently present and can influence healthy and pathologic biomechanics and ultimately clinical decision-making. Characterizing variation in bony morphology and material properties in the population can support treatment and specifically the design, via shape and sizing, of shoulder implants. Total Shoulder Arthroplasty (TSA) is the treatment of choice for glenohumeral osteoarthritis as well as bone fracture. Complications and poor outcomes in TSA are generally influenced by the inability of the implant to replicate the natural joint biomechanics and by the bone quality around the fixation features. For this reason, knowledge of bony morphology and mechanical properties can support optimal implant design and sizing, and thus improve TSA results. Statistical shape and intensity modeling is a powerful tool to represent the shape and mechanical properties variation in a training set. Accordingly, the objectives of this thesis were: 1) to develop a statistical shape model (SSM) of the proximal humeral cortical and cancellous bone; 2) to develop an SSM and a statistical intensity model (SIM) of the scapular bone. A training set of 85 humeri and 53 scapulae were reconstructed from CT scans and registered to common templates. Principal Component Analysis (PCA) was applied to the registered geometries to quantify morphological and bone properties variation in the population. For both the humerus and the scapula SSM, the first mode of variation accounted for most of the variation and described scaling. Subsequent modes described changes in the scapular plate, acromion process and scapular notch for the scapula, and in the neck angle, head inclination, greater and lesser tubercles for the humerus. Variation in cortical thickness of the humeral diaphysis was largely independent of size and statistically significant differences with ethnicity were noted. Asian subjects showed higher humeral cortical thickness with respect to Caucasians, regardless of gender. The first mode of variation in the scapular SIM described scaling in material properties distribution, with higher bone density located centrally and anteriorly in the glenoid region. The bone property maps developed for the scapular training set realistically captured inter-subject variability and they represent a valuable tool to assess fixation features and screw location and trajectories for TSA glenoid component. The SSMs and SIM developed in this thesis represent a useful infrastructure to support population-based evaluations and assess possible anatomical differences with gender and ethnicity, SSM and SIM can also provide anatomical relationship in support of implant design and sizing.

Document Type

Thesis

Degree Name

M.S.

Department

Bioengineering

First Advisor

Peter J. Laz, Ph.D.

Second Advisor

Lorenzo Patelli

Third Advisor

Paul Rullkoetter

Statistical Shape and Intensity Modeling of the Shoulder

_____

A Thesis

Presented to

the Faculty of the Daniel Felix Ritchie School of Engineering and Computer Science

University of Denver

_____

In Partial Fulfillment

of the Requirements for the Degree

Master of Science

_____

by

Irene Sintini

August 2017

Advisor: Peter J. Laz

Author: Irene Sintini
Title: Statistical Shape and Intensity Modeling of the Shoulder
Advisor: Peter J. Laz
Degree Date: August 2017

ABSTRACT

Anatomical variability in the shoulder is inherently present and can influence healthy and pathologic biomechanics and ultimately clinical decision-making. Characterizing variation in bony morphology and material properties in the population can support treatment and specifically the design, via shape and sizing, of shoulder implants. Total Shoulder Arthroplasty (TSA) is the treatment of choice for glenohumeral osteoarthritis as well as bone fracture. Complications and poor outcomes in TSA are generally influenced by the inability of the implant to replicate the natural joint biomechanics and by the bone quality around the fixation features. For this reason, knowledge of bony morphology and mechanical properties can support optimal implant design and sizing, and thus improve TSA results. Statistical shape and intensity modeling is a powerful tool to represent the shape and mechanical properties variation in a training set. Accordingly, the objectives of this thesis were: 1) to develop a statistical shape model (SSM) of the proximal humeral cortical and cancellous bone; 2) to develop an SSM and a statistical intensity model (SIM) of the scapular bone. A training set of 85 humeri and 53 scapulae were reconstructed from CT scans and registered to common templates. Principal Component Analysis (PCA) was applied to the registered geometries to quantify morphological and bone properties variation in the population. For both the humerus and the scapula SSM, the first mode of variation accounted for most of the variation and

described scaling. Subsequent modes described changes in the scapular plate, acromion process and scapular notch for the scapula, and in the neck angle, head inclination, greater and lesser tubercles for the humerus. Variation in cortical thickness of the humeral diaphysis was largely independent of size and statistically significant differences with ethnicity were noted. Asian subjects showed higher humeral cortical thickness with respect to Caucasians, regardless of gender. The first mode of variation in the scapular SIM described scaling in material properties distribution, with higher bone density located centrally and anteriorly in the glenoid region. The bone property maps developed for the scapular training set realistically captured inter-subject variability and they represent a valuable tool to assess fixation features and screw location and trajectories for TSA glenoid component. The SSMs and SIM developed in this thesis represent a useful infrastructure to support population-based evaluations and assess possible anatomical differences with gender and ethnicity, SSM and SIM can also provide anatomical relationship in support of implant design and sizing.

ACKNOWLEDGEMENTS

First, I must thank my advisor Dr. Peter Laz for his invaluable support and mentorship, inside and outside the University, and for believing in me.

I want to thank Dr. Paul Rullkoetter and Dr. Lorenzo Patelli for serving as members of my committee. I also am grateful to Dr. Rullkoetter for his valuable insights on the project and his professional guidance.

I want to thank Will Burton for his work in the scapula project. I also thank all the graduate students at the Center for Orthopaedic Biomechanics: AZ, Sean, Don, Lowell, Vasiliki, Aruna, Veronica, Brecca, Craig.

I am also grateful to DePuy Synthes for funding my project and to Paul Sade, Jason Chavarria, James Brownhill, Chad Lawrence and Kyle Secrist for providing the scan data and making sure my research was always driven by clinical questions.

Lastly, I thank Alessandro for everything.

TABLE OF CONTENTS

LIST OF TABLES

LIST OF FIGURES

CHAPTER 1. INTRODUCTION

1.1. Introduction

Uncertainty is present in many aspects of the human body, such as geometry and mechanical property, alignment, loading or kinematics (Fitzpatrick et al., 2011). Specifically, anatomical variation in the morphology and material properties of the human bones must be reconciled with a finite inventory of orthopaedic implant designs and sizes (Pearl et al., 2009). Therefore, a systematic quantification of this variation is crucial to optimize the geometry and fixation features of medical devices, ensuring that each design and each size fits the largest number of subjects in the population.

In biomechanics, computational modeling is a powerful tool that overcomes the main limitations of experimental testing, which are high costs in terms of expense and time, limited number of cadaveric specimen for *in vitro* testing, and inability to measure internal quantity *in vivo* with non-invasive techniques. Computational modeling offers an efficient infrastructure to investigate the complexity of the musculoskeletal system in various aspects, such as measuring natural joint mechanics (Ali et al., 2016), or evaluating the performance of orthopaedic implants in relation with the surrounding natural structures (Navacchia et al., 2016). Computational modeling is often implemented at a subject-specific level, which is ideal to characterize the features of the analyzed subject, but cannot provide information about how these features compare against the rest of the population.

Statistical shape and intensity modeling combines, which the advantages of computational modeling with a probabilistic approach, is well suited to investigate variations in largely scattered data as the human anatomy (Navacchia et al., 2016) and to perform population-based evaluations (Laz and Browne, 2010). Statistical shape modeling has been applied to investigate variation in bone shape (Kamer et al., 2016) or joint morphology (Baldwin et al., 2010), mechanics (Fitzpatrick et al., 2011), and kinematics (Smoger et al., 2015), as well as in the distribution of mechanical property of the bone (Bryan et al., 2010).

The work presented in this thesis is focused on the use of statistical shape and intensity modeling to describe the variability in morphology and mechanical property in the shoulder bones, i.e., humerus and scapula, with the overall goal of providing clinical information in support of the design of shoulder orthopeadic implants. The clinical questions that motivate this study are several and they are driven by the need for shoulder replacements capable of successfully restoring normal joint function. On the humeral side, the 'fit and fill' of the humeral stem component in the cancellous bone canal and replication of the head center are key considerations to optimize the outcome of the surgery and they are driven by the underlying bony anatomy. In addition, specific patterns of bony morphological and dimensional variation between genders and ethnical groups have been recognized (Gebhart et al., 2013, Darling et al., 2013, Nelson et al., 2004) and whether to differentiate implant designs based on these characteristics remains an open question. On the scapular side, the loosening of the glenoid component is a major cause of failure (Hasan et al., 2002, Robertson et al., 2017) and has been linked to bone stock quality around the

fixation features as well as to the ability of the component to match the natural glenoid surface, maximizing coverage of cortical bone.

1.2. Objectives

The objectives of this thesis were 1) to develop a statistical description of the proximal humeral morphology to quantify variation across the population, and 2) to develop a statistical description of the scapular mechanical property in conjunction with its shape to quantify variation across the population. The models were built deriving the 3D bone geometry and material property distribution from computed tomography (CT) scans of a training set of subjects and specimen of various ethnicities and both gender. Statistical analyses were performed after having consistently registered the training set to a common template. Specifically, Principal Component Analysis (PCA) (Jolliffe, 2002) was applied to quantify the anatomical variation in the training set, both in the bony shape and material property.

1.3. Thesis Overview

Chapter 2 provides an overview of the published literature on statistical shape and intensity modeling for biomechanical applications as well as a description of the glenohumeral joint natural anatomy and total shoulder arthroplasty implants.

Chapter 3 presents *Investigating Gender and Ethnicity Differences in Proximal Humeral Morphology using a Statistical Shape Model* whose objective was to develop a statistical shape model of the cortical and cancellous regions of the proximal humerus and assess potential shape differences with gender and ethnicity.

Chapter 4 presents Investigating *Assessment of Scapula Shape and Bone Quality using Finite-Element Statistical Models* whose objective was to develop a statistical description of scapular anatomy and mechanical property variation in the population to support design, sizing and placement of total shoulder arthroplasty implants.

Chapter 5 discusses the specific contributions of this thesis in addition to suggestions for application of statistical shape and intensity modeling to support design and sizing of orthopaedic implants as well as surgical planning.

CHAPTER 2. BACKGROUND INFORMATION AND LITERATURE REVIEW

2.1. Statistical Shape and Intensity Modeling

Variability of biological structures is a challenge for engineers and clinicians, who want to design medical devices and plan surgical procedure for the entire population. Variability of anatomical and biomechanical aspects, such as patient geometry, material properties, joint kinematics and loading, generates variability in orthopeadic aspects, such as implant design and component alignment, as well as clinical outcomes (Laz and Browne, 2010). Statistical shape models (SSM) and statistical shape and intensity models (SSIM) can quantify respectively the morphological and mechanical variability by describing the average bone shape and average bone density distribution together with the main modes of variation of shape and density distribution within a population (Sarkalkan et al., 2014). These statistical models are generally created based on a training set that informs the model with the expected shape and density distribution of bones (Sarkalkan et al., 2014). The ability of the models to effectively capture intersubject variability is strictly related to the size and the quality of the training set, meaning how accurately the target population is represented. SSMs have also the ability of identifying anatomical variation of a sub-population with a common background (Sarkalkan et al., 2014): for example, they can be developed for healthy individuals as well as for pathological populations, such as osteoporotic or osteoarthritic, or for subjects of a specific ethnicity or gender. Quantifying anatomical variation of the entire population or in specific sub-population can provide new

opportunities to clinicians for diagnosis, treatment and surgical planning and to engineers for medical devices design and sizing.

In medicine, patient-specific models are ideal for personalized medical treatments, but not always feasible from time and financial perspectives. SSM can potentially overcome the need for these models or, at least, reduce the high costs associated to them, specifically from a computational standpoint. In this sense, SSM have been used as predictive tools: for example, in the shoulder joint, to predict the shape of a bone from the shape of the adjoining segment (Yang et al, 2008), or in the knee, to predict various anatomical quantities, such as joint kinematics and contact mechanics, from joint shape, both on the patellofemoral (Fitzpatrick et al., 2011) and tibiofemoral (Smoger et al., 2015) side. An additional application of the SSM is the automated segmentation of medical images, such as CT scan or MRI, to efficiently and accurately reconstruct the 3D geometry of bone and cartilage, without intra- and inter-observer variability (Fripp et al., 2007, Baldwin et al., 2010, Rasoulian et al., 2013).

While SSM have been extensively presented in the literature for various bones, for example the pelvis (Lamecker et al., 2004) or the humerus (Kamer et al.,2016), and joints, for example the knee (Baldwin et al., 2010, Fitzpatrick et al., 2011, Smoger et al., 2015), the spine (Campbell and Petrella, 2016) or the shoulder (Mutsvangwa et al., 2015, Yang et al., 2008), only a limited number of studies have developed SSIM (Querol et al., 2006, Bryan et al., 2010, Nicolella and Bredbenner 2010). In addition, all these studies have focused on the femur. The general approach for developing an SSIM of the bone consists in deriving its apparent density distribution from the CT scan gray scale (Schileo et al.,

2008), and then converting these data to Young's moduli, using experimental derived relationship (Morgan et al., 2003, Gupta et al., 2004). If SSM can be used to support design and sizing of medical devices for the all population or for sub-populations that share specific morphological characteristics (Fitzpatrick et al., 2008), SSIM are crucial for testing such devices because they can be used to generate finite-element (FE) models with realistic material property distributions. FE analysis is becoming more and more needed to complement the experimental testing required on medical devices prior their commercialization, particularly in orthopaedics. For example, FE analyses can assess the stress distribution (Coteau et al., 2001) or predict fatigue life (Allred et al., 2016) in the implanted bone, alleviating the high costs and time associated to *in vivo* and *in vitro* experimental testing. In addition, FE models can provide quantitative information on how the device impacts the biomechanics of the joint, measuring all those internal quantities that are not easily measurable in experiments, such as muscles, ligaments or contact forces (Baldwin et al., 2010, Rao et al., 2013, Navacchia et al., 2016). Developing subject-specific FE models is a complex and time-consuming process and SSIM of the bone can automate parts of it (Campbell and Petrella, 2016), becoming a particularly useful tool in the medical device industry.

In general, SSM and SSIM are powerful computational infrastructures for population-based evaluations or probabilistic analyses, allowing the generation of new instances (Campbell and Petrella, 2016), to expand the original training set and explore the boundaries of anatomical variability, including best- and worst-case scenarios. The lager the training set, the more realistically the SSM and SSIM capture anatomical variations in

the population. Since variation patterns can be hard to find in data set of high dimensions, SSM and SSIM are generally created using Principal Component Analysis, a statistical tool that reduces the dimensions of the initial data set, retaining the variation present in it (Jolliffe, 2002). The following paragraph provides more details on the mathematical process behind Principal Component Analysis.

2.1.1. Principal Component Analysis

Principal Component Analysis (PCA) is a type of multivariate analysis whose goal is to reduce the dimensions of a data set, while retaining as much as possible of the variation present in it (Jolliffe, 2002). This reduction is achieved by transforming the original data to a new set of variables, the principal components (PC), which are uncorrelated, and which are ordered so that the first few retain most of the variation, i.e. the highest explained percentage of variation, present in the original variables (Jolliffe 2002). By finding the eigenvectors of the covariance matrix, PCA provides all the orthogonal, i.e. independent, modes of variation in a set of data. Each instance of the original data set becomes then a linear combination of all or some modes of variation. The covariance matrix is shown in Eq. 2.1 for a two-dimension (2D) data set.

$$Cov(X,Y) = \frac{\sum_{i=1}^{n}(X_i - \bar{X})(Y_i - \bar{Y})}{(n-1)} \qquad (2.1)$$

If the dimension of the data set is greater than two, the covariance matrix is computed as in Eq. 2.2.

$$C(X,Y,Z) = \begin{matrix} Cov(X,X) & Cov(X,Y) & Cov(X,Z) \\ Cov(Y,X) & Cov(Y,Y) & Cov(Y,Z) \\ Cov(Z,X) & Cov(Z,Y) & Cov(Z,Z) \end{matrix} \qquad (2.2)$$

The bone is a 3D object and its surface can be modeled as a point cloud or a mesh, in which each node or anatomical landmark is described by three spatial coordinates *X*, *Y*, *Z* in the Cartesian space. Therefore, to build the SSM of a bone, PCA is applied using a covariance matrix as in Eq. 2, where *X*, *Y*, *Z* are the coordinates of the nodes of each bone of the training set. Before applying PCA, it is crucial to establish correspondence between the geometries in the training set, so that each variable has the consistent meaning across the training set. This can be accomplished either manually selecting the same anatomical landmarks on each subject or using automated approaches, such as Coherent Point Drift algorithm (CPD) (Myronenko et al., 2010). CPD morphs a template geometry to the subject's shape and establishes nodal correspondence through a nearest-neighbor search, selecting, for each node of the morphed template, the closest node on the subject's mesh. In case of SSIM, the covariance matrix must account for a fourth dimension, i.e. density or Young's modulus of each node. The eigenvectors of the covariance matrix represent the orthogonal direction along which the data vary the most. Eigenvalues λ and eigenvectors *v* are defined as in Eq. 2.3 and can be computed using Eq. 2.4.

$$Cv = \lambda v \qquad (2.3)$$

$$|(C - \lambda I)| = 0 \qquad (2.4)$$

In case of the SSM of a bone or a joint, after applying PCA, the modes of variation can be visualized by transforming back the data from the PC space to the Cartesian space. A common way to do this is constructing the mean geometry and adding to it a certain amount of standard deviation for one PC at the time. This approach allows to differentiate the effect of each PC on shape variation.

2.2. The Glenohumeral Joint

The glenohumeral joint is one of the four joints that comprise the shoulder. It is classified as a synovial or diarthroidal joint, being surrounded by a joint capsule filled with synovial fluid. The glenohumeral joint articulates the humeral head, which is located on the proximal part of the humerus, to the glenoid cavity, which is located on the lateral side of the scapula (Figure 2.1). It is considered a ball and socket joint, however, the socket, i.e. the glenoid cavity, has large radii of curvature in both the coronal and transverse plane, providing the joint with minimal geometrical constraint. In fact, the humerus and the scapula are allowed 6 degree-of-freedom (DoF) with respect to each other: ab/adduction, internal and external rotation, flexion and extension, as well as translations in all the three directions. The most common surgical intervention to treat osteoarthritis or pain in the glenohumeral joint is Total Shoulder Arthroplasty (TSA), with consists in replacing the damaged articular surfaces with artificial component. The following paragraphs provide a brief overview on the glenohumeral joint anatomy and the Total Shoulder Arthroplasty.

2.2.1. Anatomy

As the glenoid cavity has a much higher radius of curvature than the humeral head (Figure 2.1), the glenohumeral joint derives most of its stability from the surrounding soft tissue (Kelkar et al., 2001). The joint capsule and the ligaments of the glenohumeral joint provide the passive restraint needed to keep the humeral head in contact with the glenoid cavity. Three ligaments can be identified in the joint: the superior and middle ligaments, that originate in the glenoid and insert in the anatomical neck of the humerus, and the

inferior ligament, that originate in the glenoid and insert at the lesser tuberosity of the humerus (Wolf et al., 1995, Steinbeck et al., 1998).

In addition to the ligaments and the capsule, the shoulder muscles and tendons have a crucial role in providing stability the joint; specifically, the primary active stabilizers of the glenohumeral joint are known as the rotator cuff. The rotator cuff is comprised of the following muscles: supraspinatus, infraspinatus, teres minor and subscapularis (Clark et al., 1992, Reddy et al., 2000); these muscles also contribute significantly to the articular movement, specifically to ab/adduction and internal and external rotation.

The bones that comprise the glenohumeral joint are the humerus and the scapula. The humerus is classified as a long bone, having a shaft (diaphysis) which is longer than it is wide, with epiphyses at both the proximal and distal end; it presents a hard outside compact shell known as cortical bone and a softer spongy internal structure known as cancellous bone (Figure 2.2), containing bone marrow. The epiphyses of the humerus are covered in cartilage, in correspondence of the articulations with the adjoining segments. On the other hand, the scapula is a flat bone and it still presents the same cortical and cancellous bone type (Figure 2.2). The scapula is composed by a flat plate (shoulder blade), the glenoid cavity and two processes: the coracoid and the acromion (Figure 2.1); the superior border of the plate usually presents a notch (Figure 2.1).

2.2.2. Total Shoulder Arthroplasty

TSA involves replacing damaged articular surfaces with artificial components (Figure 2.3). Per the American Academy of Orthopaedic Surgeons, 53000 TSA surgeries are performed each year in the United States, making TSA the third most common total

joint replacement, after the hip and the knee. Several pathological conditions can lead to this type of intervention, such as glenohumeral osteoarthritis, rotator cuff arthropathy or severe bone fracture, usually on the humeral side. The goal of TSA is to alleviate pain and to restore normal function of the joint in terms of mobility and strength. Currently, two different designs exist for TSA (Figure 2.3): the anatomic design, in which the humeral head replicates closely the natural humeral anatomy, and the glenoid is resurfaced with a polyethylene component, and the reverse design, where the glenoid component is convex and the humeral stem has a proximal concave head (Sanchez-Sotelo, 2009). The reverse design is indicated in case of massive rotator cuff tear, i.e. muscular weakness, because it can improve the joint function by increasing the moment arm of the deltoid muscle (Walker et al., 2016). A larger moment arm will facilitate the abduction movement, decreasing the required muscle force to generate torque. In both designs, the humeral component presents a stem that should fit inside the intramedullary canal of the humerus.

Although TSA is in general an effective procedure, with successful results reported in over 90% of the cases Hasan et al. (2002), patient dissatisfaction and necessity for revision surgeries are still a concern that needs to be addressed. Stiffness and instability are the main complaints, while glenoid loosening is the major cause of failure in TSA, accounting for 59% of cases according to (Hasan et al., 2002). After glenoid loosening, the main causes of failure are humeral head malposition or humeral head loosening and rotator cuff tears (Hasan et al., 2002, Deshmukh et al., 2005). Complications and poor outcomes in TSA are influenced by the ability of the implant to replicate the natural joint biomechanics and the bone quality. For this reason, knowledge of bony morphology and

mechanical properties can potentially improve implant design and sizing, and thus improve TSA results.

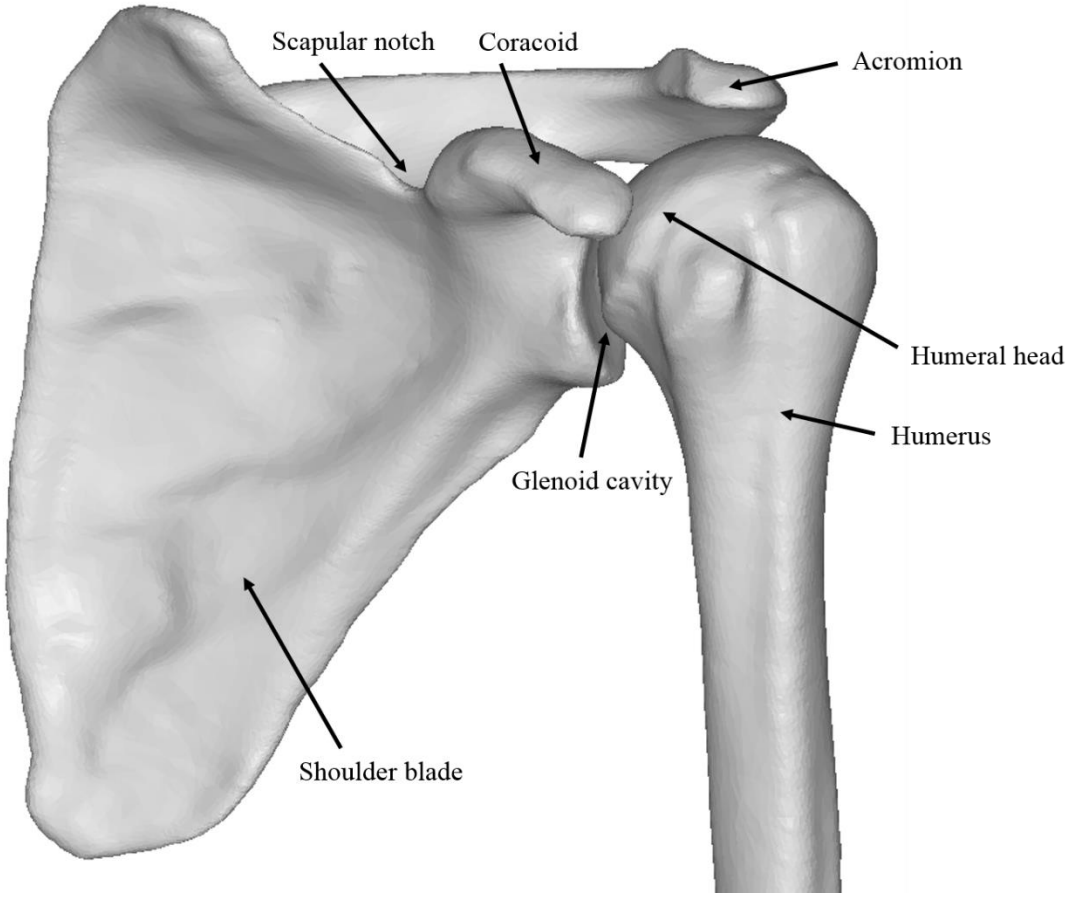

Figure 2.1 Articular 3D geometry of the glenohumeral joint.

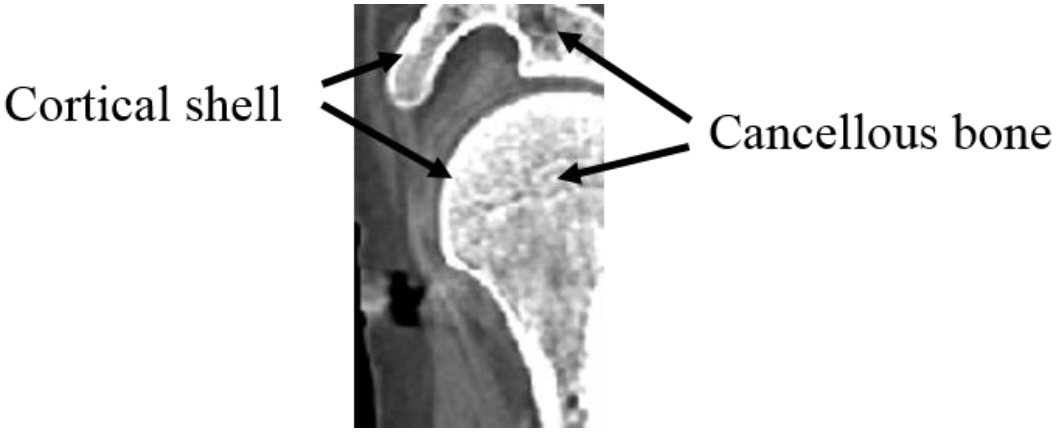

Figure 2.2 Frontal section of the glenohumeral joint from CT scan: cortical bone is the thick white shell on the outside boundary while cancellous bone is the lower-density bone in the internal area.

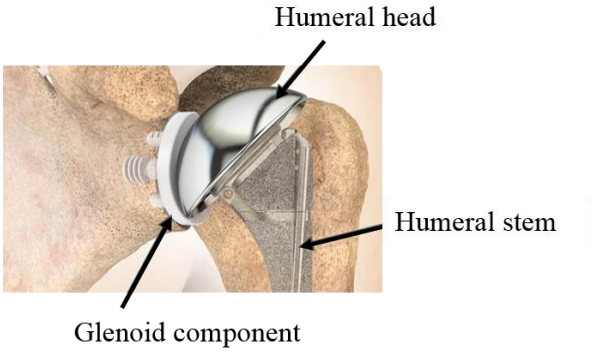

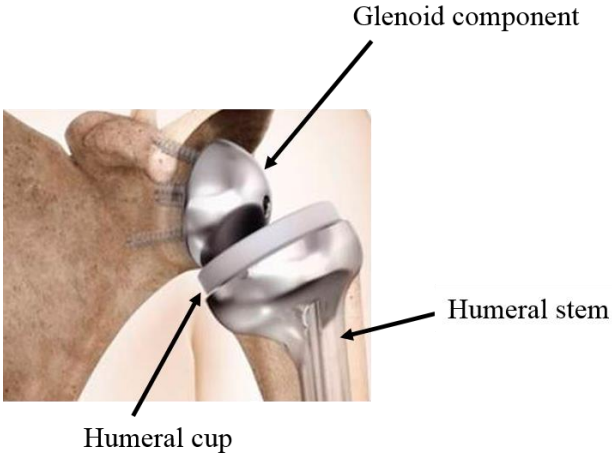

Figure 2.3 Examples of anatomic (top) and reverse (bottom) implant design for Total Shoulder Arthroplasty (DePuy Synthes).

CHAPTER 3. INVESTIGATING GENDER AND ETHNICITY DIFFERENCES IN PROXIMAL HUMERAL MORPHOLOGY USING A STATISTICAL SHAPE MODEL

3.1. Abstract

Morphological variability in the shoulder is inherently present and can influence healthy and pathologic biomechanics and ultimately clinical decision-making. Characterizing variation in humeral morphology in the population can support treatment and specifically, the design, via shape and sizing, of shoulder implants. Accordingly, the objectives of this study were to quantify proximal humeral geometry and to assess whether shape variation was influenced by gender and ethnicity. A statistical shape model (SSM) of the proximal humeral cortical and cancellous regions was developed for a training set of 85 subjects, comprised of both genders and different ethnicities (Asian, Caucasian, African American). Cortical and cancellous bony geometries were reconstructed from CT scans, meshed with triangular elements and registered to a template. Principal component analysis was applied to the registered geometries to quantify modes of variation in the training set. Clinically relevant anatomical measurements were computed on the registered geometries to assess correlation with modes of variation. Specific regions of interest included the humeral head, intramedullary canal and the orientation of the canal relative to the head center. Parallel analysis was performed to identify which principal components or modes of variation were significant. Parallel analysis identified six significant modes of variation. The first six modes accounted for more than 93% of the variation in the training set,

describing scaling (Mode 1), inclination of the head (Mode 2, 5), and shape of the greater tuberosity and neck region (Modes 3-6). Statistically significant differences with gender, where female subjects were smaller than males, were observed in Mode 1; however, no other differences were observed in subsequent modes. Statistically significant differences in thickness of the diaphyseal cortical shell were observed with ethnicity; Asian subjects had larger cortical thickness compared to similar-sized Caucasian subjects. The statistical description of cortical and cancellous bone humeral morphology and quantified differences with ethnicity provide important descriptive data to support surgical planning and improve implant design for the world population.

3.2. Introduction

The anatomy of the proximal humerus inherently influences the biomechanics of the shoulder and plays a direct role in various clinical scenarios, such as bone fractures and total shoulder arthroplasty (TSA). In the natural shoulder, the proximal humeral anatomy defines the glenohumeral conformity, and rotator cuff, muscle and soft tissue attachments, which influence muscle moments, motion and overall stability of the joint. Proximal humerus fractures are common injuries and the morphology of the bone has direct implications for nonoperative treatment, internal and external fixation, and hemiarthroplasty (Sanchez-Sotelo, 2006). In complex facture cases, models of bones can be used to align bone fragments and guide the surgical repair (Doerfler et al., 2017, Schumann et al., 2016).

The current study, however, is motivated by describing the natural anatomy in the context of TSA to assess and improve implant design. The demand for TSA has rapidly

grown during the past decades, causing a likewise increase in revision surgeries, which tend to be more complex than primary arthroplasties (Day et al., 2010). Despite the high success rate of this surgical procedure, complications in TSA are not rare and about 30% of the revision surgeries performed from 1996 to 2005 were caused by instability of the glenohumeral joint (Bohsali et al., 2006). In TSA, "fit and fill" of an implant in the humeral canal and replication of the head center are key considerations to optimize the outcome of the surgery and they are driven by the underlying bony anatomy. Humeral head curvature determination is also important when choosing the appropriate head size and alignment in TSA procedures (Gebhart et al., 2013).

Variation in humeral anatomy has been investigated to support clinical decision-making and implant design based primarily on 2D measurements from medical images (Ballmer et al., 1993, Boileau and Walch, 1997, DeLude et al., 2007, Hertel et al., 2002, Humphrey et al., 2016, Pearl et al., 1996, Pearl et al., 1999, Pearl et al., 2009, Robertson et al., 2000). These studies identified a largely scattered anatomy (Hertel et al., 2002), which must be reconciled with a finite prosthetic inventory (Pearl et al., 2009). Specifically, variation in the dimensions of the head, the relative position of the center of the head on the shaft, and the diameter of the intramedullary canal have been explored with the purpose of evaluating and optimizing implant design, sizing and placement. While the placement is customized on the patient, a finite number of implant designs and sizes must fit the entire population. Thus, a quantitative understanding of how the humeral shape changes throughout the population is essential to support implant design and sizing.

Statistical shape modeling (SSM) have been applied to quantify morphological variations of bones, including femur and tibia (Bredbenner at al., 2010, Bryan et al., 2010, Galloway et al., 2013), and pelvis (Lamecker et al., 2004). Following registration of the training set geometries to a common template, principal component analysis (PCA) is applied to the covariance matrix of the registered data to describe the independent modes of variation (Joliffe, 2002). Further, as the geometries are registered to a template, the approach allows for the automated and consistent computation of anatomical measurements across large sets of data. Therefore, statistical shape modeling represents a suitable frame to evaluate current implants and to inform new designs in regard to the natural bone anatomy.

SSM have been previously developed for the entire shoulder joint (Mutsvangwa et al., 2015, Yang et al., 2008) and for the proximal humerus only (Drew et al., 2014, Kamer et al., 2016). Mutsvangwa et al. developed methods to assess the shape of the humerus and scapula for a training set of 28 human subjects (Mutsvangwa et al., 2015), while Yang et al. proposed a similar work for 28 primates (Yang et al., 2008). Recently, Kamer et al. (2016) developed a statistical model that included information on both morphology and bone quality for a population of proximal humeri (58 subjects). These studies described shape variability of the external cortical shell only, and did not directly consider the morphology of the cancellous region or the potential impact of ethnicity or gender, which is valuable from surgical and implant-design perspectives. Drew et al. (2014) considered the intramedullary canal shape, developing an SSM of the cortical humeral bone boundaries on the endosteal and periosteal surfaces. However, this statistical model was

based on a population of only 10 subjects, which limits the broad applicability of the results.

As implants are designed to function for the population, differences in 3D anatomy with gender and ethnicity have previously been investigated. A gender-dependent size difference was identified in the medial meniscus (Vrancken et al., 2014), with Caucasian males being larger than Caucasian females, and in the knee (Mahfouz et al. 2012), with males being larger than females regardless of ethnicity (Caucasians, Asians, African Americans). Specific patterns of morphological variation have been recognized among ethnicity groups for the tibia (Darling et al., 2013) and for the femur (Nelson et al., 2004). These studies reported that postmenopausal Caucasian women had statistically significantly larger tibiae and lower tibial bone density and cortical thickness, compared to Asian women (Darling et al., 2013), as well as lower femoral bone strength and thinner femoral neck cortices, compared to African-American women (Nelson et al., 2004). In a regression model of the proximal humerus, gender was identified as one of the variables influencing humeral head curvature; other factors included epicondylar breadth, height, and humeral length (Gebhart et al., 2013). However, a systematic SSM-based analysis of how gender and ethnicities might influence the proximal humeral shape has not yet been performed. Accordingly, the objectives of this study were: 1) to develop a SSM to quantify shape variation in both cortical and cancellous bone regions of the proximal humerus, 2) to investigate correlations between the 3D shapes and common anatomical measurements of the proximal humerus, and 3) to assess potential shape differences with gender and ethnicity.

3.3. Methods

The training set comprised 85 left humeri of healthy subject and cadavers (age: 75 ± 14 years, 38 females and 47 males) and included 52 Caucasian, 31 Asian and 2 African American subjects. Bones were classified as healthy if they did not present any abnormal morphological feature or sign of joint diseases, such as osteophytes. CT scans were performed with nominal settings: tube voltage 130 KvP, tube current 22 Ma, slice thickness 1 mm and pixel spacing 0.49. The study made use of CT scans from cadavers and subjects enrolled in other studies and was classified as exempt by our institutional review board (IRB). The 3D geometries of the cortical and cancellous regions were reconstructed from CT scans using ScanIP (Simpleware, Exeter, UK) (Figure 3.1). The diaphysis of each bone was resected at a length proportional to its head radius (5.6 times), because the proximal bone was the region of interest for this study and the entire humerus was not available for the entire training set. The resection length was chosen to preserve the portion of the diaphysis of interest for TSA stems. Three-node triangular surface meshes were generated for each cortical and cancellous bone using Hypermesh (Altair Engineering, Troy, MI), with an average element size of 1.0 mm. A median geometry (male, Caucasian, head radius: 24.4 mm) was selected as the template and used to create an anatomical coordinate system, which was defined per ISB recommendations (Wu et al., 2005). The template was selected as it was among those geometries that included the distal portion of the bone, providing the full set of landmarks required to construct the anatomical coordinate system. The origin was placed in the glenohumeral rotational center, estimated as the center of the best-fitting sphere for the humeral head; the mediolateral axis was defined by the direction

of the segment connecting the two epicondyles; the anterior-posterior axis was defined as the perpendicular to the plane of the glenohumeral rotational center and the epicondyles; the superior-inferior axis was defined consequently to form a right-hand coordinate system.

Training set geometries were registered to the template using the process as follows (Figure 3.1Figure 3.1 Statistical shape modeling workflow. Bone geometries were reconstructed from CT scans; cortical and cancellous bones were meshed and registered to a template.). The cortical geometries were rigid-body aligned to the cortical geometry of the template using an iterative closest point algorithm (Besl and McKay, 1992). The rigid-body transformation matrix obtained for each cortical bone was then applied to the respective cancellous bone as well, in order to preserve the original relative position of the two surface meshes. After the alignment, nodal correspondence was established using a coherent point drift algorithm (Myronenko et al., 2010), first morphing the template geometry onto the subject geometry and then performing a nearest-neighbor search for each node of the morphed template to the nodes of the subject. For this approach to function well, it was essential that the subject mesh was considerably finer than the template mesh (average element lengths: 2.5 mm). After nodal correspondence was established, each geometry was rigid-body transformed so that the origin was placed in the center of the head and the superior-inferior axis was coincident with the axis of the intramedullary canal. Head center and canal axis were computed using respectively, a best-fitting sphere and a best-fitting cylinder, with a least-square type of algorithm. This orientation was chosen because it is meaningful from both surgical and implant-design perspectives. By performing the transformation after nodal correspondence was established, an automated

transformation process could be applied using consistent node numbers for the head and canal regions.

The SSM was created by applying PCA to the registered data, which consisted of nodal coordinates (x, y, z) for the cortical and cancellous geometries for all the registered subjects. Modes of variation described the anatomic variation present in the population, and each instance was represented as a series of principal component (PC) scores. A leave-one-out (LOO) analysis was performed to assess the accuracy of the SSM in predicting the shape of an unseen subject. A parallel analysis was performed (Horn, 1965) to identify how many modes of variation were meaningful, i.e. not noise. Clinically relevant anatomical measurements were computed automatically for each registered bone. Head radius was computed from the best-fitting of the humeral head. Canal diameter was computed as the minimum diameter of a series of four inscribed circles in the cancellous bone sections at 10, 20, 30 and 40 mm above the most distal section of the shaft. Outer diameter of the cortical bone was computed from the best-fitting cylinder of the external surface of the lower portion of the shaft (70% of the length). Cortical thickness in the humeral shaft was computed as the average radial distance between the cortical and the cancellous profile, at multiple sections of the shaft, from 35 to 90 mm (about 25% to 75% of the length of the mean subject, measured from the head center) below the head center. Further, medial and posterior offset, greater tuberosity offset, inclination angle and articular thickness were computed as in previous studies (Boileau and Walch, 1997, Hertel et al., 2002). Anatomical measurements and PC scores were analyzed via Pearson's correlation coefficient (R) and, by gender and ethnicity, via unpaired Student's t-test.

3.4. Results

Morphological changes in the cortical and cancellous proximal humerus were defined as a series of modes of variation (Figure 3.2). Parallel analysis identified six significant modes of variation. The first six modes of variation explained more than 93% of the total variation present in the training set and they were visualized by perturbing the mean geometry at ± 2.5 standard deviations of each principal component (PC). Mode 1 largely described uniform scaling, i.e. scaling of the head size in conjunction with the outer diameter and shaft length of the bone (71.6% of variation explained); Mode 2 (9.5%) and Mode 5 (2.6%) described changes in the head shape and orientation in the surgical neck area; Mode 3 (4.1%), Mode 4 (3.1%) and Mode 6 (2.1%) described various changes in the region of the greater tubercle and of the surgical neck area (Figure 3.2). Observations of the modes for the cortical bone (Figure 3.2) are mirrored in the cancellous bone (Figure 3.2). The LOO analysis assessing the ability of the SSM to represent an unforeseen subject resulted in an absolute geometric error of 0.48 mm (std. dev.: 0.16 mm) averaged across all nodes and all subjects. Parallel analysis identified 6 meaningful modes of variation.

Several correlations between modes of variations and anatomical measurements (Table 3.1 Pearson's correlation coefficients (R) between PC scores and anatomical measurements. High correlations (R>0.65) are bold.), and between anatomical measurements were observed (Table 3.2). Mode 1 was strongly correlated with head radius (R=0.95) and outer diameter (R=0.88), but only moderately correlated with canal diameter (R=0.51) and cortical thickness (R=0.50). Mode 1 was also strongly correlated with articular thickness (R=0.86) and greater tuberosity offset (R=0.87). Head radius was highly

correlated with outer diameter (R=0.76) but only moderately correlated with canal diameter (R=0.45) (Figure 3.3, Table 3.2). Mode 2 was strongly correlated with medial offset (R=-0.79) and head inclination angle (R=0.66). Mode 3 was moderately correlated with head inclination angle (R=0.52) and Mode 4 was moderately correlated with the anterior-posterior offset (R=0.40) and the canal diameter (R=-0.45). Mode 5 was moderately correlated with the medial offset (R=-0.57). Means, standard deviations and ranges of the anatomical measurements are shown in Table 3.3

Gender and ethnicity differences were primarily described by scaling. Statistically significant differences were observed in Mode 1 for gender (unpaired Student's t-test, $p<4e-12$) and ethnicity ($p<0.02$), but not in subsequent modes. Statistically significant differences were observed for head radius between gender and ethnicities (Figure 3.4, Table 3.4) for medial offset between ethnicities (Table 3.4). Variation in cortical thickness of the diaphysis was largely independent of size (Figure 3.5) and statistically significant differences with ethnicity were noted for average cortical thickness computed between 35 and 90 mm below head center (Asian vs. Caucasian, $p<0.05$). At similar head sizes, Asian subjects showed higher cortical thickness, regardless of gender (Figure 3.5). No statistically significant differences with ethnicity were found for the canal diameter (Figure 3.6), but they were found with gender ($p<0.01$).

3.5. Discussion

An SSM of the proximal humerus was developed to describe the three-dimensional shape of the cortical and cancellous bone regions of 85 subjects. The morphological variation across the population was systematically quantified using PCA, which represents

a state-of-the-art technique to assess the most important anatomical variations (Kamer et al., 2016). Most of the variation (71.6%) could be attributed to the size of the bone (Mode 1), whereas subsequent modes of variation involved pure shape changing in the head inclination and surgical neck region (Mode 2, 5), and in the greater tubercle region (Modes 3, 4, 6). Gender-dependent differences were observed in Mode 1 only, i.e. gender affects the size of the bone but not its shape. Ethnicity-dependent differences were observed in Mode 1, i.e. ethnicity affects the size of the bone, and in the cortical thickness, i.e. Asians subjects had higher thickness than Caucasians. Anatomical measurements were in good agreement with previous studies (Boileau and Walch, 1997, Hertel et al., 2002, Humphrey et al., 2016), confirming that the SSM is a technique to automatically, accurately and consistently compute measurements on large dataset.

The first six principal components explained more than 93% of the total variation present in the training set, with the first one alone accounting for 71.6% of variation. The results affirm that PCA was performed on geometries that were properly aligned with respect to each other. Thus, modes of variations described actual shape variability between subjects and not noise due to inconsistent alignment. As expected, the first mode of variation described scaling for both the cortical and cancellous bone regions. Interestingly, the first mode of variation was strongly correlated with the radius of the head and the outer diameter, which represent the size of the bone, but less correlated with the diameter of the canal (Figure 3.3). This finding demonstrated that the internal and external diameters of the humeral shaft do not scale uniformly. Functional analysis, e.g. through finite element modeling, is required to assess how the shape variation impacts the joint biomechanics

(Vrancken et al, 2014) and it can be performed on geometries generated from the SSM through clustering analysis, to minimize the computational cost while maintaining a good representation of the variation in the population. Clustering analysis can be applied to the data represented as PC scores (Ding and He, 2004), in order to subdivide the dataset into groups that maximally differ from each other (Vrancken et al., 2014). The number of clusters can be assigned equal to the number of modes of variation that parallel analysis identified as significant or it can be optimized using gap-statistics (Vrancken et al., 2014).

The training set included subjects of both genders and three different ethnicities, thus allowing the identification of common anatomical patterns in sub-populations with the same characteristics. Differences between males and females were primarily in size, as in (Humphrey et al., 2016), with male subjects being larger than females. Statistically significant differences between genders were present in the first mode of variation ($p<4e-12$). No statistically significant differences were observed in subsequent modes, which implies that there are no shape differences (beyond scaling) attributed to gender.

With regard to ethnicity, the first mode of variation also presented differences, although less significant for ethnicity (Asian vs. Caucasian, $p<0.04$) than gender. Our analysis (Table 3.4, Figure 3.5) suggested that there are no significant differences between Asians and Caucasians in terms of outer and canal diameter but there are significant differences for cortical thickness (note that cortical thickness was not calculated simply as the difference between the two diameters. Cortical thickness in the diaphysis exhibited differences with ethnicity ($p<0.04$) and with gender ($p<0.001$) too. In general, larger cortical bone thicknesses in the diaphysis and smaller humeral head radii were observed

for the Asian population compared to the Caucasian population (Figure 3.5). This result agrees with a previous study (Darling et al., 2013), which suggested that Asian women may compensate for smaller tibiae with an increased cortical thickness, with respect to Caucasian women. Quantitative information on cortical thickness variation in the population is important for implant design since this parameter influences implant sizing and stability. The implication of the canal diameter varying independent of outer diameter (R=0.56, from Table 3.2) requires implant systems to consider combinations of stems sizes with head designs and offsets to accommodate variations observed in the population, specifically with regard to both stem fit and biomechanics (e.g. replicating head center) similarly to what has been proposed for the knee joint (Hovinga and Lerner, 2008, Mahfouz et al., 2012). In addition, statistically significant differences were found for medial offset, with Asians having larger offset than Caucasians (Table 3.4).

Specific regions of interest for the humeral bone included the humeral head and the intramedullary canal, whose dimensions and relative orientation can inform TSA head sizing, stem design and offsets to facilitate replication of the native anatomy and to assess load transfer and stability. The statistical shape model allows for an automated calculation of many clinically-relevant anatomical measurements (Boileau and Walch, 1997, Hertel et al., 2002). This aspect is not only convenient from a time perspective, but also ensures consistent measurements across the subjects. Statistically significant differences were found between Asian and Caucasian subjects in the radius of the head, but not in the diameter of the canal (Table 3.4); this observation suggests that Asian subjects were

smaller in size and their cortical thickness did not scale at the same rate as for Caucasian subjects.

Statistical shape modeling has been used to quantify variation in the proximal humerus shape (Kamer et al., 2016); however, the shape of the cancellous bone in relationship to the outside morphology of the bone has not been investigated, except for a limited number of subjects (10 subjects in Drew et al., 2013). The diameter and general curvatures of the intramedullary canal are crucial dimensions from an implant design perspective since the humeral stem must fit inside it and match its curvature on the neck region. By capturing 3D surfaces, the SSM approach has major advantages in capturing the anatomy over using 2D distance and angle measurements. Captured in Mode 2, changes in head inclination angle represented a second important way in which the proximal humeral geometry changed across the population. This angle affects the mediolateral position of the head center with respect to the canal axis, as well as the curvature of the surgical neck region. Results from PCA suggest that TSA implants might have to accommodate these anatomical differences, allowing for various inclination angles of the head with respect to the stem.

It is important to note that the findings of the study are dependent on the training set. In the current work, the SSM was developed from CT scans of 85 subjects, which while larger than prior SSM work (Mutswanga et al., 2015, Kramer et al., 2016, Yang et al., 2008), could be expanded to strengthen the work. The ethnicity distribution included 52 Caucasians, 31 Asians, 2 African Americans and was thereby not fully representative of the global population. With the ability to characterize 3D variation in anatomy, the SSM

platform is well suited to investigate anatomical differences with gender and ethnicity and inform the sizing and design of TSA implants, specifically because PC were interpreted with regard to typical clinical measures.

In closing, a statistical shape model approach characterized the variability in proximal humerus morphology and accurately captured both cortical and cancellous bone anatomy. While gender differences were attributed to scaling, differences in canal diameter and cortical thickness were present with ethnicity. The descriptive data will be valuable in supporting surgical planning and improving TSA implant design for the world population.

3.6. Tables and Figures

Table 3.1 Pearson's correlation coefficients (*R*) between PC scores and anatomical measurements. High correlations (*R*>0.65) are bold.

	PC1	PC2	PC3	PC4	PC5	PC6
Head Radius	**0.95**					
Greater Tub. Offset	**0.87**			0.17		-0.15
Medial Offset		**-0.79**	-0.29	0.26	-0.57	
Ant.-Post. Offset	-0.22	0.34	0.24	0.40		
Art. Surf. Thickness	**0.86**			0.19		
Canal Diameter	0.51	-0.15		-0.45		0.16
Inclination		**0.66**	0.52	-0.28		-0.15
Outer diameter	**0.88**	-0.11		-0.28		
Cortical Thickness	0.50			0.12		

Table 3.2 Pearson's correlation coefficients (R) between anatomical measurements. High correlations (R>0.65) are in bold.

	Radius	GTO	MO	APO	ATC	Canal Diameter	Inclination	Outer Diameter	Cortical Thickness
Radius	1								
GTO	**0.84**	1							
MO	-0.09	0.17	1						
APO	-0.13	-0.14	-0.3	1					
ATC	**0.84**	**0.83**	0.03	-0.06	1				
Canal Diameter	0.45	0.28	-0.01	-0.36	0.26	1			
Inclination	-0.12	-0.16	**-0.7**	0.23	-0.06	-0.11	1		
Outer Diameter	**0.76**	**0.71**	0.1	-0.35	**0.67**	0.56	-0.05	1	
Cortical Thickness	0.16	0.31	011	-0.06	0.29	-0.46	0.05	0.35	1.0

Table 3.3 Mean and standard deviation of the anatomical measurements computed on the population.

	Mean ± St. dev.	Range
Radius (mm)	24.1 ± 2.5	19.3 – 29.4
Greater tuberosity offset (mm)	40.1 ± 3.6	33.1 – 47.8
Medial Offset (mm)	6.3 ± 2.4	0.8 – 16.4
Anterior-posterior offset (mm)	-1.9 ± 1.3	-4.4 – 4.4
Articular surface thickness (mm)	19.0 ± 1.7	15.5 – 22.5
Canal Diameter (mm)	12.1 ± 2.1	7.3 – 17.6
Inclination (°)	136.5 ± 4.4	111.5 – 144.8
Outer Diameter (mm)	23.1 ± 2.5	18.7 – 28.6
Cortical Thickness (mm)	3.6 ± 0.8	2.1 – 5.7

Table 3.4 Unpaired Student's t-test results (p value) for anatomical measurements and PC scores with gender and ethnicity (n.s.= not significant, if p>0.05). Only quantities that showed significant differences were reported.

	Gender	Ethnicity
PC1	4e-12	0.02
Head Radius	3e-11	6e-4
Outer Diameter	2e-16	n.s.
Canal Diameter	0.01	n.s.
Medial Offset	n.s.	0.02
Cortical Thickness	1e-4	0.04

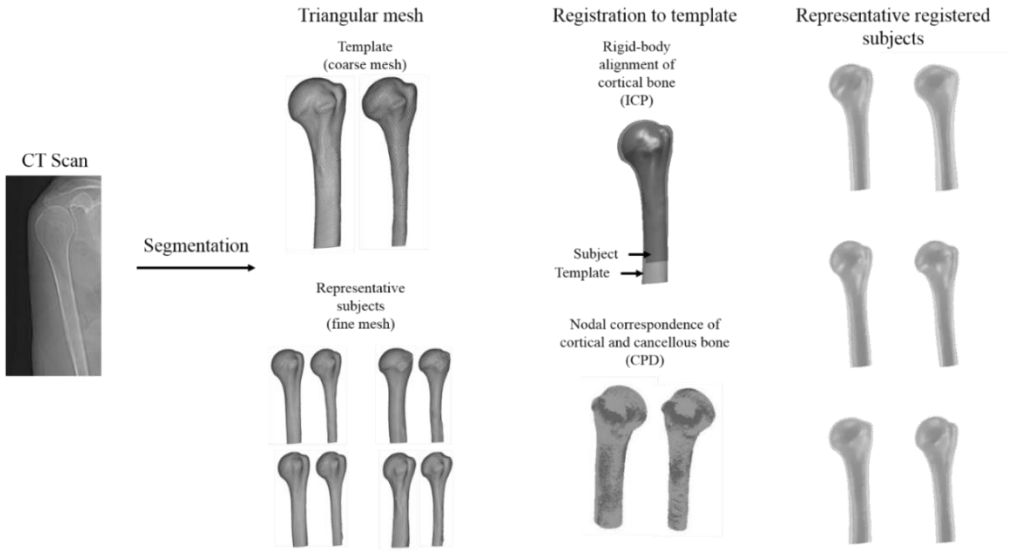

Figure 3.1 Statistical shape modeling workflow. Bone geometries were reconstructed from CT scans; cortical and cancellous bones were meshed and registered to a template.

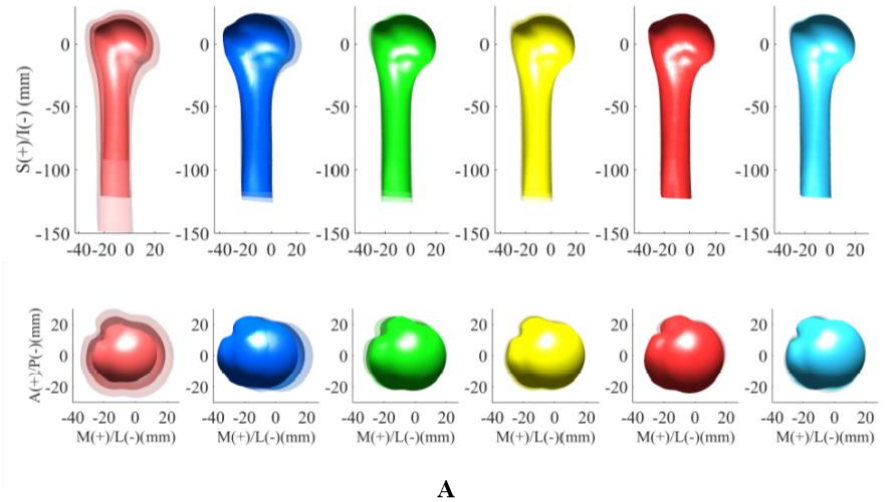

A

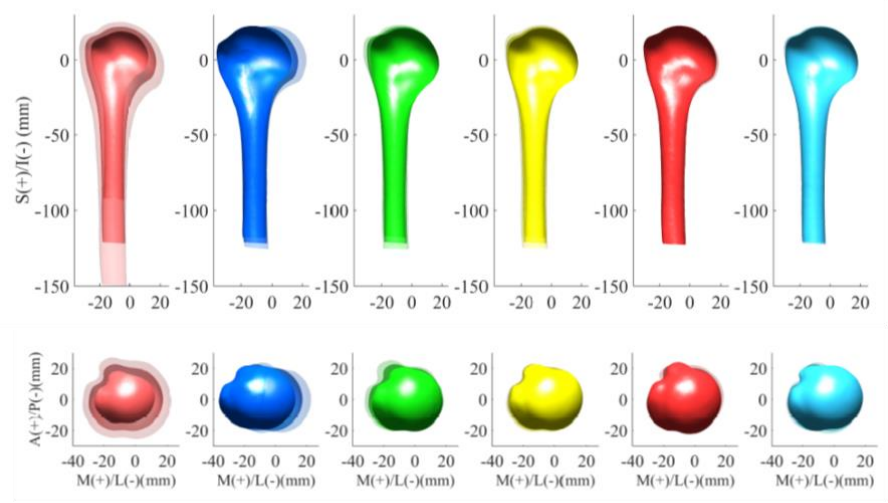

B

Figure 3.2 Shape of cortical (A) and cancellous (B) bone for the first six PC modes of variation (shown at ± 2.5 std. dev. from the mean) in sagittal (top) and transverse (bottom) plane.

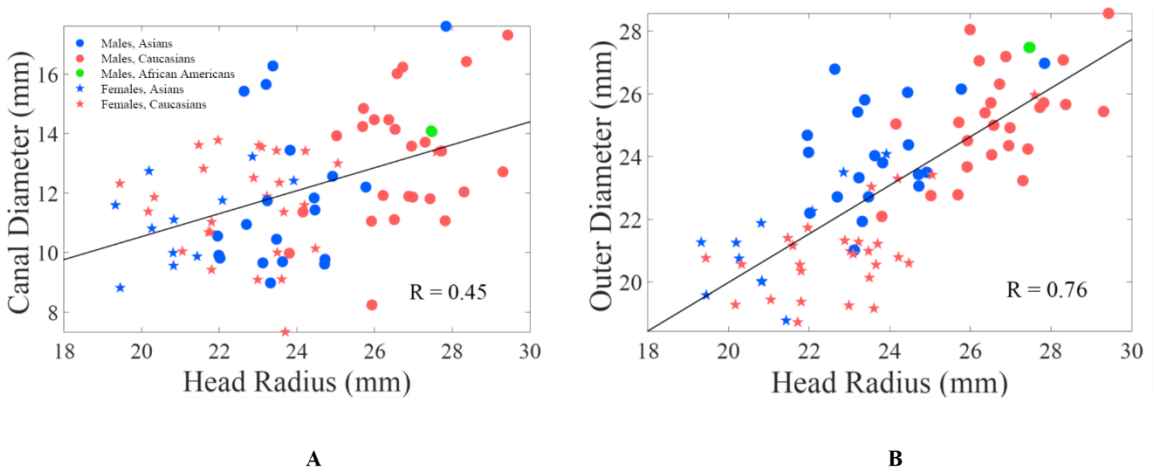

Figure 3.3 Relationships for head radius vs. canal dimeter (A) and outer diameter (B).

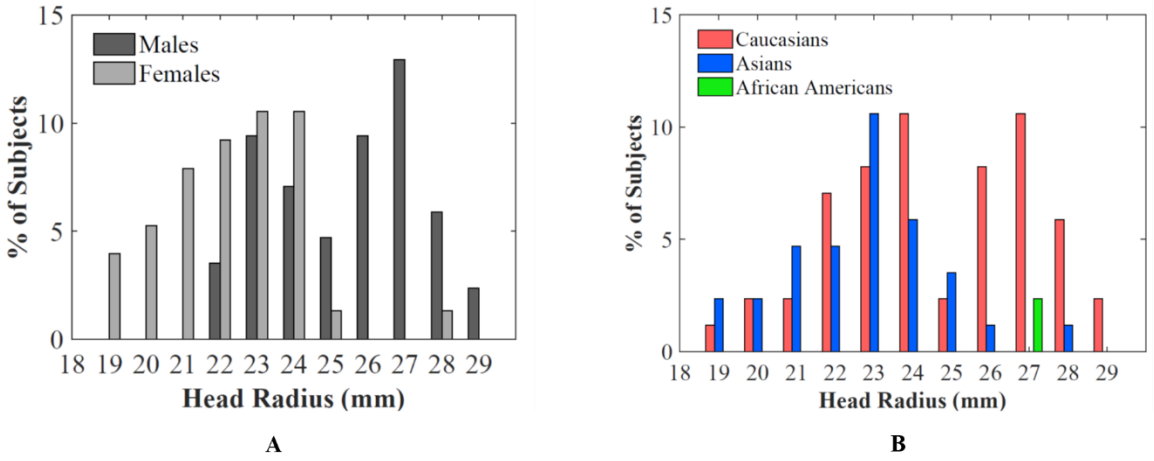

Figure 3.4 Distribution of head radius for gender (A) and ethnicity (B). Percent of subjects is calculated with respect to the entire population.

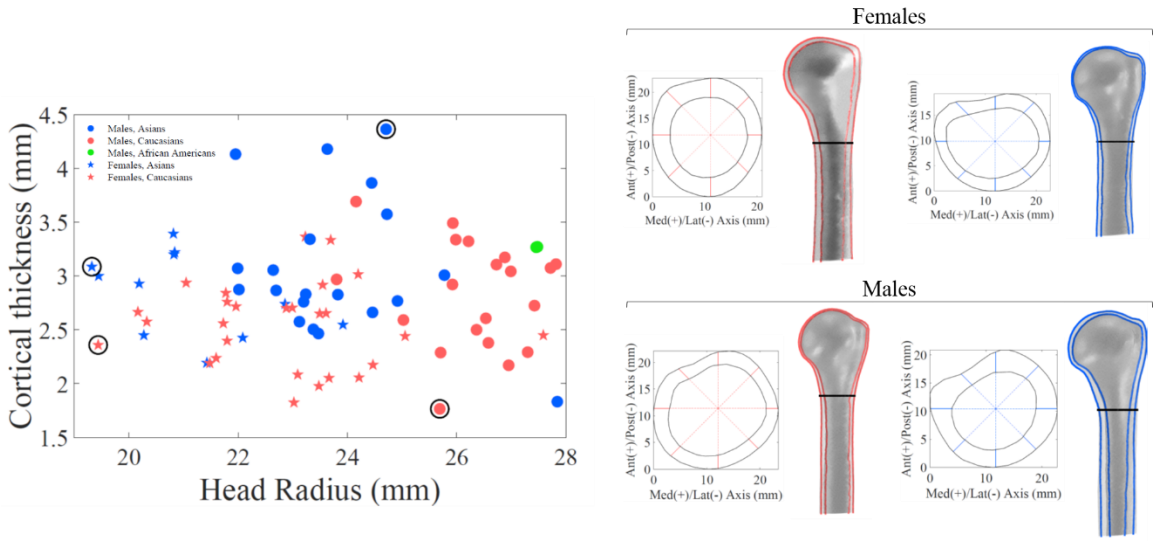

Figure 3.5 Relationships for head radius and average cortical thickness (35 mm below head center). Bone profiles for representative (circled) Caucasian and Asian subjects.

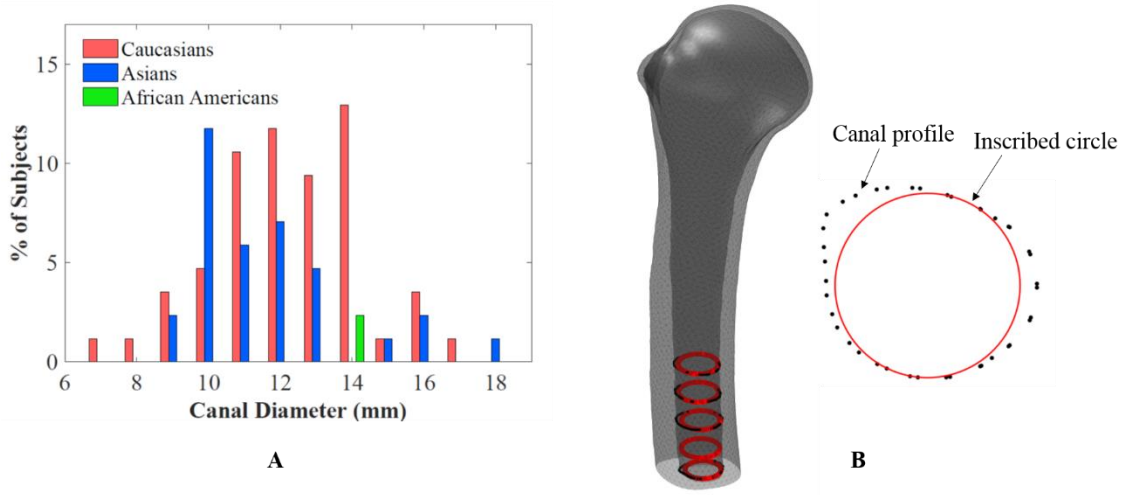

Figure 3.6 Canal diameter distribution for the population (A). Canal diameter was computed as the minimum diameter of a series of inscribed circles (red lines) in the cancellous shaft sections (black dots), between the most distal section and a section 40 mm proximal to it, every 10 mm (B). Statistically significant differences were not found between Asians and Caucasians.

CHAPTER 4. ASSESSMENT OF SCAPULA MORPHOLOGY AND MATERIAL PROPERTY USING A FINITE ELEMENT STATISTICAL SHAPE AND INTENSITY MODEL

4.1. Abstract

Knowledge of shape and material property variability in the scapula can inform total shoulder arthroplasty. Prior studies assessed scapular shape through measurements on cadaveric specimens and on computed tomography (CT) scans, and through statistical shape models. Scapular material properties have been evaluated through cadaveric testing and CT scans. However, most studies were limited to few subjects. The objective of this study was to develop statistical models to quantify variation of scapular anatomy throughout the population. A population of 53 material-mapped finite-element models of healthy scapulae was reconstructed from CT scans and registered to a common template. A statistical shape model (SSM) and a statistical intensity model (SIM) were developed using Principal Component Analysis to describe respectively morphological and material properties variation. The first three modes of variation of the scapula SSM described: scaling (Mode 1, 54% of variation); changes in medial border and acromial process (Mode 2, 9%); elongation of scapular blade (Mode 3, 7%). Mode 1 of the SIM (43% of the variation) described scaling of bone quality in central glenoid. A mild correlation (R=0.41) was observed between the first shape and intensity modes. Higher bone quality was consistently observed in the central glenoid. SSM and SIM have implications for implant design and sizing. Results from SSM and SIM presented respectively uniform bone scaling

and contrast in bone quality distributions in central and inferior glenoid as the primary modes of variation. Larger scapula size was not strongly linked to better bone quality.

4.2. Introduction

While total shoulder arthroplasty (TSA) is in general a successful procedure, complications due to loosening of the implant in the glenoid remain the main cause of failure. Glenoid loosening has been noted as the cause for 52% of 154 cases of TSA revisions (Roberson et al., 2017) and 59% of 139 cases (Hasan et al., 2002) of unsatisfactory TSA. Glenoid loosening is influenced by the inability of the implants to replicate the natural joint anatomy and biomechanics as well as by the quality of the bone surrounding the fixation features of the glenoid component (Matsen et al., 2008).

Knowledge of the morphological variability in the scapula throughout the population can inform the design and sizing of TSA implants. Previous studies characterized the glenoid dimensions by manually taking measurements from computed tomography (CT) data (Matthews et al., 2017, Fulin et al.,2017), analyzing reconstructed 3D geometries (Frankle et al., 2009, Ghafurian et al., 2016), or measuring cadaveric specimens (Merrill et al., 2001, Churchill et al., 2001). The time-consuming processes associated with taking manual measurements, and the intrinsic limitation of using two-dimension (2D) measurements to characterize the shape of the three-dimensional (3D) bone geometry, can be overcome with statistical shape modeling (SSM). SSM is a mathematical tool that, through Principal Component Analysis (PCA), reduces the size of a given set of data, while retaining all the variation present in it. This is accomplished by representing every subject of a training set as a vector of Principal Components (PC), each

of which describes an orthogonal, i.e. independent, mode of variation of the population. In this way, SSM allows for a systematic quantification of the shape variation present in a training set of geometries or in sub-population that share common features, such as ethnicity, gender, or pathological status (Fitzpatrick et al., 2008). Prior studies have described morphological variations of various bones and joints with SSMs (Smoger et al., 2015, Fitzpatrick et al., 2011) but not many have focused on the shoulder. One study developed an SSM of the glenohumeral joint using 28 primate shoulders, which included the scapula and humerus (Yang et al., 2008) and other recent studies have developed automated workflows for SSM and applied them to the human scapula (Mutsvangwa et al., 2015, Mayya et al., 2013).

If knowledge of morphological variation is required for optimal implant design and sizing, characterizing the internal material property distribution of the glenoid vault, as well as how these distributions vary throughout the population, can inform the location and trajectories of the glenoid component's fixation features, such as the peg and the supplemental screws (Kalouche et al., 2010). Prior studies have assessed the underlying bone quality in various regions of the glenoid through mechanical testing of the human glenohumeral joint (Mansat et al., 1998, Frich 1994, Mimar et al., 2008, Anglin et al., 1999). However, limitations in mechanical testing are due to sparsity in data and difficulty of sampling. On the other hand, it has been shown that material mapped finite-element (FE) models based on CT scan data provide accurate representations of material properties and allow for finely mapped material data (Keyak et al., 2001, Schileo et al., 2008). Studies have characterized localized material properties in bones through a regression-based

approach that relates Hounsfield units (HU) to apparent density (Gupta et al., 2004). In order to develop FE models, apparent density is converted to Young's modulus using bone-specific relationships derived from mechanical testing (Morgan et al., 2003, Frich 1994). If material properties are collected for a training set of bones, they can be incorporated into the SSM to generate statistical shape and intensity models (SSIM), still applying a PCA approach. SSIM have been successfully developed to describe anatomic variation in shape and mechanical properties of the femur across the population (Bryan et al., Nicolella et al., 2012, Querol et al., 2006, Waarsing et al., 2010). On the other hand, statistical appearance or intensity models (Cootes et al., 2004, Campoli et al., 2014) can be used to quantify changes in material properties only, independently from the shape. When statistical intensity models (SIM) are developed in conjunction with SSM, potential correlation between morphology and quality of the bone can be assessed. This type of workflow not yet been implemented to quantify anatomical variation in the scapula across the population.

In addition to systematically quantifying anatomical variation in bones and joints, SSM, SSIM and SIM can be used to generate large populations of instances for probabilistic studies, i.e. Monte Carlo simulations, or specifically sampled instances that cover large portions of the population for design of experiment. New instances are generated by perturbing the modes of variation by adding or subtracting a certain amount of standard deviation of the PC to the mean geometry (Campbell and Petrella, 2016). This type of workflow has implications in the design and sizing of implants that must fit the entire population (Laz and Browne, 2010). Accordingly, the objectives of this study were 1) to develop an SSM and an SIM of the scapula to explore the variation in shape and

material properties distribution throughout the population, assessing potential correlation between bone size and bone quality, and 2) to develop an SSM of the glenoid region to explore only the anatomical variation in the main region of interest for implant placement.

4.3. Methods

Scapular geometries for a training set of 53 healthy subjects and cadavers (26 males, 27 females, age mean: 73, st. dev.: 14) were segmented from CT scans using ScanIP (Simpleware, Exeter, UK) (Figure 4.1). The bones did not show any sign of osteoarthritis or deformity. CT scans were performed on two identical machines, with the following protocol: tube voltage 120-140 KvP, based on the size of the subject, tube current 22 Ma, slice thickness 0.5-1.25 mm. Our IRB classified the study as exempt as it made use of existing CT scans from subjects enrolled in other studies and cadavers. Surface meshes were generated for each subject using Hypermesh (Altair Engineering, Troy, MI), with an average element size of 1.0 mm. A median geometry was chosen as the template to which the other geometries were registered. The template was represented in its anatomical coordinate system as per (Wu et al., 2005), with the difference that the origin was placed in the center of the glenoid, which is a more relevant location from a TSA perspective. The template surface mesh was represented by 16,384 nodes and 32,762 triangular (tri) elements (Figure 4.1). Surface mesh registration was an iterative process performed in MATLAB (Mathworks, Natick, MA) by morphing the template mesh to take on the shape of the subjects. An iterative closest point (ICP) algorithm was used to rigidly align the subject geometries to the template. Note that we refer to scans from both living subjects and cadavers as ‘subjects’, to distinguish them from the template. Then, coherent point

drift (CPD) (Myronenko et al., 2010) was iteratively performed on the template to conform the template to the subject meshes. The CPD algorithm allowed for global scaling, skewing, translation, rotation, and local deformation. Given the highly irregular scapular geometry, subsequent to the CPD algorithm, a non-rigid iterative closest point (ICP) algorithm (Besl and McKay, 1992) was performed on the template to further morph the template mesh to take on each subject's shape. As a result of this iterative morphing workflow, the template surface mesh fully conformed to each subject surface mesh, thus yielding a registered training set of surface meshes. The surface registered training set was necessary for registration of volumetric meshes. The surface mesh of the template was filled with four-node tetrahedral (tet) elements to create a 3D template mesh (Figure 4.1). The tet template mesh consisted of 42,839 nodes and 204,208 four-node tet elements, with element side lengths ranging from 1.0 to 1.4 mm. 3D registration was performed by elastically deforming the template tet mesh to the subject tri mesh, using the known displacements between the subjects' registered surface nodes and corresponding surface nodes on the template. The elastic deformation process was implemented using finite element software (Abaqus SIMULIA, Providence, RI); in each simulation, the nodal displacements were set as boundary conditions. This was performed for all 53 subject geometries and yielded a population of 53 3D registered scapulae.

PCA was applied to the registered surfaces in order to create an SSM of the entire scapula to explore the morphological variability throughout the population. Additionally, PCA was applied to a sub register of only glenoid nodes in order to create an SSM of the glenoid, as this is the main region of interest for the placement of TSA glenoid components.

Modes of variation were described by perturbing the mean geometry by ± 2 standard deviations of each principal component (PC). A Leave-One-Out (LOO) analysis was performed to assess the capability of the SSM to reconstruct a subject from its PC (Smoger et a., 2015). A parallel analysis was performed (Horn, 1965) to identify how many shape modes of variation were meaningful, i.e. not noise. Clinically relevant anatomical measurements were computed on the registered geometries. Glenoid height was computed as the long axis of the best-fit ellipse of the glenoid profile in the sagittal plane, while glenoid width was computed as the diameter of the best-fit circle of the inferior portion of the glenoid profile in the sagittal plane. Glenoid retroversion and inclination angles were calculated as in (Friedman et al., 1992, Matsumura et al., 2014, Ghafurian et al, 2015) and in (Churchill et al, 2001, Werner et al., 2017), respectively. Glenoid radii of curvature in the coronal and transverse plane (McPherson et al., 1997) were calculated from best-fit circles, using a least-square algorithm.

Material mapped FE models were generated based on original CT scan data of the geometries. Each subject was meshed with element side lengths between 0.5 to 1.0 mm using ScanIP's meshing algorithm. Then, each material mapped FE model was overlaid on corresponding CT data in order to associate each element with underlying CT pixels. The tet meshes with element side lengths between 0.5 and 1.0 mm were generated using ScanIP's meshing algorithm for each segmented scapula geometry. CT scans had been performed using consistent machine settings and a CT calibration phantom (QCT Pro, Mindways Software, Inc., Austin TX) had been included in order to derive the relationship

between cancellous bone mineral density (ρ) and greyscale values, i.e. HU. The following calibration equation was used to convert Hounsfield units to bone mineral density:

$$\rho_{QCT} = 0.0006782\,HU - 0.009409 \qquad (^{gr}/_{cm^3})$$

Bone mineral density was converted into apparent density using the following relationships (Schileo et al., 2008):

$$\rho_{ash} = \frac{\rho_{QCT} + 0.09}{1.14} \qquad (^{gr}/_{cm^3})$$

$$\rho_{app} = \frac{\rho_{ash}}{0.598} \qquad (^{gr}/_{cm^3})$$

Because of surface artifact complications, apparent density of all elements with at least one node on the surface was set based on the maximum HU for that CT scan mask. Surface artifact refers to the issue where the error of the scapular geometry mask causes CT pixels that lie outside the scapula in the CT slice to be accounted for in determining material properties (Figure 4.2). This causes the material properties of the cortical elements to be inaccurate. Furthermore, this correction is justified as the internal material properties, not the cortical bone, were the focus of this study. The other exception to the relationship between HU and apparent density was a lower bound set on the apparent density. One of the reasons for the inclusion of a lower bound was the occurrence of surface artifact in the scapular mask. CT pixels included in the scapular mask that lay outside of the scapula were low enough to yield a negative apparent density based on the relationship between HU and density. Cancellous bone density was converted to Young's Modulus using the following

scapular-specific relationship, which was derived from mechanical testing (Frich, 1994) and validated in a previous study (Gupta et al., 2004).

$$E = 0.001049\rho^2 \qquad \rho \leq 350\ Kg/m^3$$

$$E = 3\times10^{-6}\rho^3 \qquad \frac{350\ Kg}{m^3} \leq \rho \leq \frac{1800\ Kg}{m^3}$$

The material mapped FE models had material properties assigned to each element, but the nature of the SSIM required material properties to be associated to each node. Therefore, elements and corresponding material properties from the ScanIP models were represented by elements' centroids. This point cloud of centroids with material properties was overlaid on its corresponding tet registered subject. A nearest-neighbor search was performed in order to associate each registered node with the material property of the centroid that lays closest to it. As a result, each registered node was associated with its apparent density. The SIM was created by performing PCA on the material properties of the registered nodes of 53 subjects. Similar to the SSM, modes of variation were described by perturbing the mean material distribution by ± 2 standard deviations of the first PC and a LOO analysis was performed to assess the capability of the SIM to reconstruct the material properties of a subject from its PC. The Student's t-test was applied to assess potential statistically significant differences with genders and the first mode of variation of the SIM and the SSM A parallel analysis was performed (Horn, 1965) to identify the number of meaningful modes of variation in the SIM. PCA was also applied to a register composed by the coordinates of both the internal and surface nodes of the registered scapulae. The geometries generated perturbing the modes of variation of this SSM were super-imposed

with the material properties distribution generated perturbing the modes of variation of the SIM, with the goal of understanding the boundaries of variation in scapular anatomy.

4.4. Results

Scapula SSM

The first three modes of variation of the whole scapula SSM accounted for nearly 70% of variability in the training set (Figure 4.2). Mode 1 (54% of variation explained) described primarily uniform scaling. Mode 2 (9%) described changes in the medial border of the plate and the acromial process. Mode 3 (7%) described a superior-inferior elongation of the scapular blade. Statistically significant differences were found between genders for SSM PC1 ($p<1.2e-4$), with males being larger than females, and PC2 ($p<0.01$). Mode 1 demonstrated strong correlation with glenoid height (R=0.82) and glenoid width (R=0.77). Mode 5 (5.5% of variation explained) demonstrated mild correlation with scapular retroversion (R=-0.45). From LOO analysis, absolute geometric errors averaged 0.94 mm (st. dev.: 0.28 mm) across all nodes and subjects. Parallel analysis identified 7 meaningful modes of variation in the SSM.

Glenoid SSM

The first three modes of variation of the glenoid SSM accounted for more than 87% of variability in the glenoid geometry (Figure 4.3). Mode 1 (62%) described changes in size, with glenoid height and width scaling uniformly. Mode 2 (19%) and mode 3 (7%) described different type of non-uniform scaling. Person's correlation coefficients of R=0.87 and R=0.78 were found between the first PC scores (PC 1) and the glenoid anterior-

posterior width and superior-inferior height, respectively. A correlation of R=0.33 was found between PC 1 and the glenoid radius of curvature from the best-fitting sphere. Glenoid width, height, retroversion angle, inclination angle, and radii of curvatures in the coronal and transverse plane are reported in Table 4.1 as mean, standard deviation and range.

Scapula SIM

The first four modes of variation of the SIM accounted for nearly 62% of variation, with Mode 1 (Figure 4.4), which accounted for 43% of variation, described a scaling of bone density in the central-anterior and inferior glenoid area, in conjunction with a dimensional scaling of the bone. Only a mild correlation (R=0.41) was found between PC1 of SIM and PC1 of SSM. No statistically significant differences were found for SIM PC1 between genders (p=0.24). From LOO analysis, absolute errors on apparent density averaged 117.5 Kg/m^3 (st. dev.: 23.2 Kg/m^3) across all nodes and subjects. Parallel analysis identified 4 meaningful modes of variation in the SIM. Figure 4.5 shows an overlay of bony material property generated from the SIM on geometries generated from the SSM built on both the internal and surface nodes.

Cancellous bone density in the glenoid region had a mean density of 377 Kg/m^3 (std. dev.: 102 Kg/m^3) across all the subjects (Table 4.2), while cortical done density had a mean of 1674 Kg/m^3 (std. dev.: 155 Kg/m^3) across all the subjects, ranging from 1421 to 1929 Kg/m^3. Cancellous bone Young's modulus in the glenoid region averaged 365 MPa (std. dev.: 263 MPa) across all the subjects (Table 4.2).

4.5. Discussion

The main purpose of this study was to provide a statistical description of morphology and mechanical properties of the scapula across the population. A series of statistical models of the whole scapula and the glenoid region were developed for a training set of 53 subjects of both genders, three different ethnicities and an average age of 73 (st. dev: 14). PCA represents a state-of-the-art technique to describe anatomical variation (Kamer et al., 2016) and, in this study, it was used to describe and quantify the variation in the scapular anatomy, including morphology and bone quality (Figure 4.2, Figure 4.3, Figure 4.4). As expected, most of the anatomical variation was captured in the first PC of the scapular SSM (54%), the glenoid SSM (62%), and the scapular SIM (43%), and it can be described as geometrical scaling and differences in regional bone quality contrast. Evaluating variation in bone quality resulted into a lower explained percentage of the first mode of variation, meaning that bone quality presents a higher anatomical variability with respect to bone shape. Perturbing the mean model by 2 standard deviations of a PC made it possible to visualize the bounds of anatomical variation for 95% of the population for that PC (Figure 4.2, Figure 4.3, Figure 4.4). This aspect makes the statistical models developed in this study useful from a clinical perspective as well as from an implant design perspective. In addition, the results from LOO analyses confirmed that the statistical models developed in this study could properly described scapular shape and material properties variation in the population.

Comparing the bone density distributions at mean ± 2 standard deviations of SIM PC 1 revealed difference in the contrast between the central, anterior, and inferior glenoid

bone quality (Figure 4.4). Interestingly, we did not find a high correlation (R=0.41) between the first SSM and SIM modes of variation, meaning that a large scapula is not necessarily linked to higher bone quality. Since bone shape and density were found to be largely independent from each other, a practical application of the SIM and SSM would be to overlay material properties distributions generated with the SIM on various bone shapes generated with the SSM (Figure 4.5). This approach could help identifying the boundaries in the scapula anatomy when designing shoulder implants.

For TSA implants, the glenoid represents a main region of interest and loosening of the glenoid component remains the main complication for this procedure (Roberson et al., 2017, Hasan et al., 2002). The loosening is influenced by the ability of the implant to reproduce natural biomechanics, and, additionally, the quality of the glenoid bone surrounding the fixation feature of the TSA component plays a key role (Matsen et al., 2008). The description of the shape and orientation of the glenoid anatomy for the population can inform implant design and sizing, and the bone property maps can support screw placement and orientation, particularly for reverse shoulder designs. Material properties in the glenoid cancellous bone were highly scattered throughout the training set, suggesting that design implants that fit large portions of the population is a challenge. The population was classified into four different groups based on where the best bone quality i.e. highest density and Young's modulus, was found, resecting the glenoid 1.5 mm below the external bone surface. The majority of the population (26 subjects) showed highest bone quality in the anterior glenoid region; 22 subjects showed highest bone quality in the central glenoid region; only 1 subject showed highest bone quality in the posterior glenoid

region; 3 subjects showed low bone quality throughout the entire glenoid. Observing these groups and the number of subjects in each group yields intuition about where the best bone quality is likely to be in a given glenoid. In general, we found that, if present, the best bone quality was consistently located in the central or anterior region of the glenoid, supporting the location of fixation features in current implants. Additionally, visualization of Mode 1 of the SIM, which describes differences in contrast in bone quality in the glenoid central and inferior regions, revealed that the central peg, as well as the anterior and inferior screws, may be crucial in glenoid fixation. Because the central, anterior, and inferior regions of the glenoid have the most variability in bone quality, based on Mode 1, the fixation features located in these regions may have varying rates of success.

The CT-based computational approach provides a finer mapping of bone properties compared to experimental mechanical testing on specimens (Mansat et al., 1998, Frich et al., 1997), with discretization dependent on scan resolution and mesh size. Mean cancellous glenoid properties were similar but slightly higher than the values reported in previous studies that explored material properties through mechanical testing (Kalouche et al., 2010, Mansat et al., 1998, Frich et al., 1997). Mansat et al., 1998 reported mean glenoid cancellous apparent densities of 274 to 302 kg/m^3 for individual subjects with values in the range of 189 to 482 kg/ m^3. Kalouche et al., 2010 reported mean glenoid cancellous apparent densities of 279 to 326 kg/m^3 for individual subjects with values ranging from 138 to 479 kg/m^3. Frich et al., 1997 reported mean cancellous apparent densities of 340 ± 100 kg/m^3 in the glenoid bare area and 380 ± 110 kg/m^3 in the superior and inferior glenoid regions. We found a mean glenoid cancellous apparent density of 377 ± 102 kg/m^3 across

all subjects, with values in the range of 243 to 596 kg/m^3. Minor incongruences may also be due to differences in the definition of the glenoid as a separate region from the entire scapula. Our values were more in line with the apparent density values reported in CT scan-based study, such as Frich, 1994 in which the glenoid mean apparent density was 380 kg/m^3.

The approach we chose to cortical material properties represented a limitation of this study. Surface artifact was corrected for by assigning all surface tet elements the bone apparent density that corresponded to the highest greyscale value found within the subject's scan. This inherently assumes that cortical properties are homogenous for the subject. However, the variability of the cortical properties across the subjects was taken in consideration and, to the authors' knowledge, only one other study (Lehtinen et al., 2004) provided this type of information for a population of 20 specimens. The cortical densities of the training set ranged between approximately 1400 and 1900 Kg/m^3, which is consistent with literature data on scapular cortical bone properties (Gupta et al., 2004, Lehtinen et al., 2004). Additionally, the discretization associated with finite elements' representation limited the ability to describe cortical shell thickness in the registered models. Cortical thickness was assumed to be the thickness of the outer layer of tet elements in the model. In reality, cortical thickness may be different throughout subjects and even depend on location in a subject. However, the focus of the study was to describe the variability in the distribution of cancellous bone properties.

The training set used to develop our statistical models was larger than that of any other statistical study performed on the scapula. All subjects and the specimens in the

training set were healthy. Future studies may explore larger populations as well as develop training sets for non-healthy subjects that are of interest from a TSA perspective, such as osteoporotic or osteoarthritic population.

Calculation of anatomical measurements was automated by taking advantage of known node identifiers from registered meshes. Glenoid height and width are important for implant design as the target for the glenoid component of the prosthetic is to replicate the native bone geometry, maximizing coverage. For this reason, knowledge of how the glenoid measurements vary may inform implant sizing. Knowledge of glenoid radii of curvature provides similar functions. Replicating the natural radius of curvature in the glenoid component may help to restore the natural kinematics of the shoulder after TSA. In general, automated computation of anatomical measurements may be more time-efficient than manual processes and potentially more consistent, as manual measurement methods may have inter- and intra-observer differences. On the other hand, consistency of automated computation of anatomical measurements using registered geometries may depend on robustness of registration.

In this study, measurements of glenoid height were slightly higher than literature. Automated computed measurements returned mean glenoid height of 45.3 mm. One study reported a mean glenoid height of 33.8 mm for females and 37.0 mm for males (Merrill et al., 2009). Another study reported mean glenoid height of 32.6 mm for females and 37.5 mm for males (Churchill et al., 2001). However, differences compared to literature may lie in how the glenoid height was computed, i.e. we computed the glenoid height as the long axis of the best-fitting ellipse on the glenoid surface. Measurements of glenoid width are

more consistent with literature. Churchill et al., 2001 reported mean glenoid width of 23.6 mm for females and 27.8 mm for males. Merrill et al., 2009 reported mean glenoid width of 23.7 mm for females and 28.56 mm for males. We found a mean glenoid width of 28.9 mm. Computed glenoid width values may be more consistent with literature as a result of more similar measurement approaches. Inclination values were similar to that reported by literature. One study reported inclination angles of 8.9 ± 9.9 degrees when computed from 3D reconstructed computer models based on CT data (Werner et al., 2017). Other literature reported inclination angles of 4.0 ± 3.4 degrees for men and 4.5 ± 3.8 degrees for women (Churchill et al., 2001). The range of retroversion angles that we found, i.e. from -3.8 to 20.1 degrees, fell within the ranges reported in the literature. Friedman et al., 1992 reported a retroversion range of -14 to 12 degrees for healthy subjects. Other studies report more narrow retroversion distributions, such as -9 to 13 degrees (Matsumura et al., 2014) and 15.1 ± 10.6 degrees for measurements based on 3D reconstructed computer models (Werner et al., 2017). Ghafurian et al., 2016 reported mean retroversion angles of -5.05 ± 3.50 degrees. The computed radii of curvature were slightly higher than what is reported in the literature. McPherson et al., 1997 reported inferior-superior radii curvature of 32.2 ± 7.6 mm and anterior-posterior radii of curvature of 40.6 ± 14 mm. We found inferior-superior radii curvature of 62.6 ± 53.4 mm, i.e. radius of curvature in the coronal plane, and anterior-posterior radii of curvature of 53.5 ± 28.1 mm, i.e. radius of curvature in the transverse plane. These differences in radii of curvature may be due to the approach taken in obtaining these values, as the referenced study depended on the identification of

continuous analytical surfaces determined on roentgenograms, whereas the approach of this paper looked at best-fitting circles to discretized point clouds.

One of the unique strengths of this study is that all the geometries in the training set are tetrahedral meshed and therefore are ready to be used in finite-element simulations of natural and implanted bone models. In the future, the SSM and SIM platform can be linked with virtual implantation of TSA implants and finite element modeling to support population-based assessments of load transfer and fixation.

4.6. Table and Figures

Table 4.1 Glenoid measurements.

	Mean ± St. dev.	Range
Height (mm)	45.3 ± 4.3	36.4-54.4
Width (mm)	28.9 ± 3.5	22.7-39.4
Retroversion (°)	6.5 ± 5.6	-4.6-19.8
Inclination (°)	3.5 ± 0.1	2.9-13.3
I-S rad. of curvature (mm)	43.4 ± 10.9	26.0-75.7

Table 4.2 Cancellous bone properties in the glenoid.

	Mean ± St. dev.	Range
Density (Kg/m3)	377 ± 102	243-596
Young's modulus (MPa)	365 ± 263	125-991

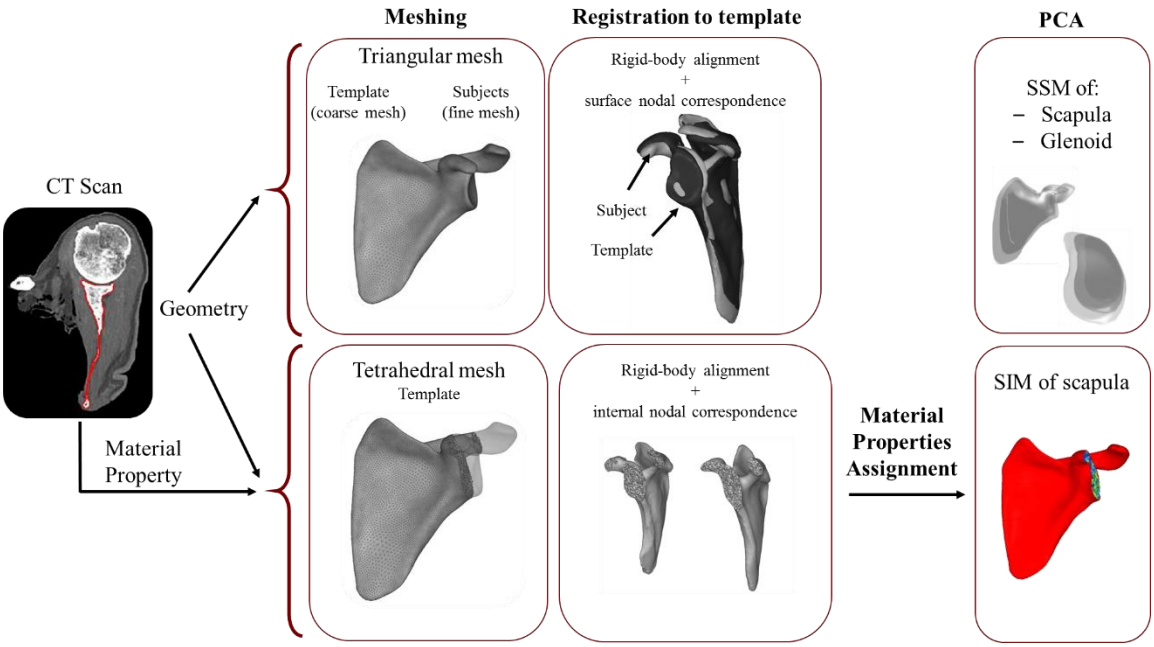

Figure 4.1 Workflow. Bone geometries were reconstructed from CT scans; all subjects were meshed with triangular elements and a template geometry was also meshed with tetrahedral elements. Surface and internal nodal correspondence between all subjects and the template was established prior performing PCA.

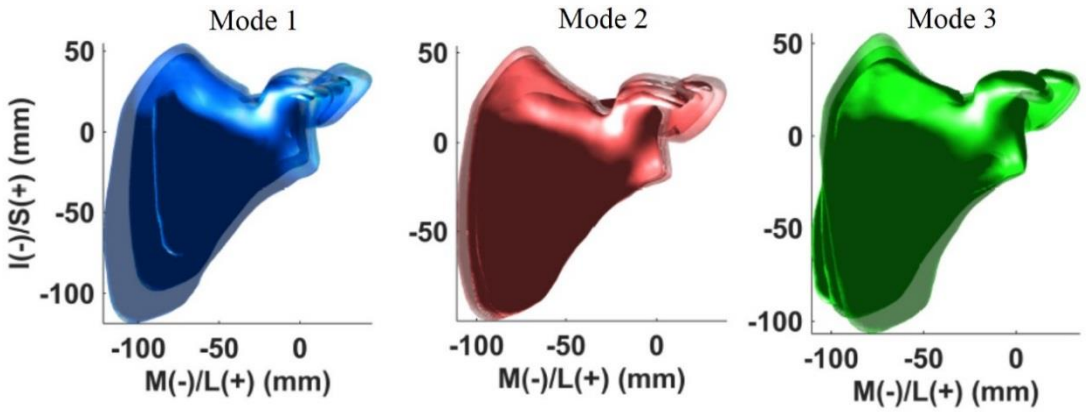

Figure 4.2 Scapula SSM. First three modes of variation are shown at mean ± 2 st. dev.

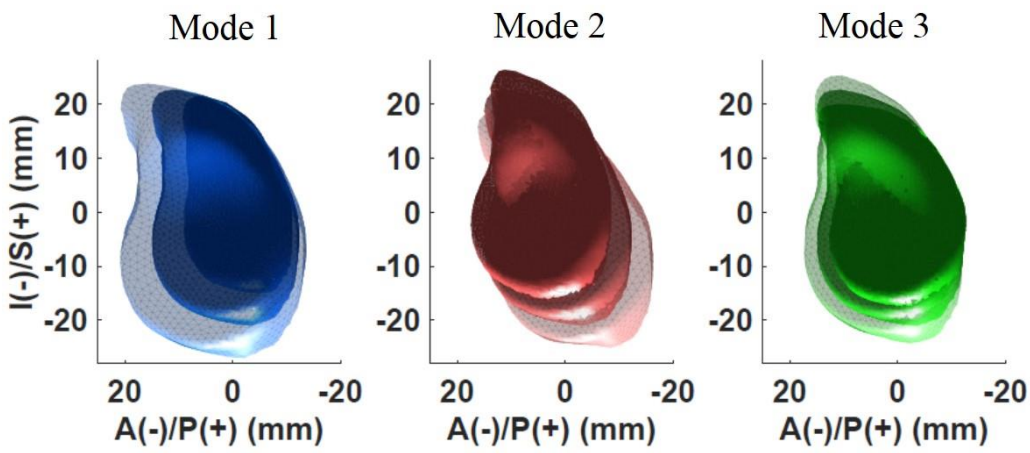

Figure 4.3 Glenoid SSM. First three modes of variation are shown at mean ± 2 st. dev.

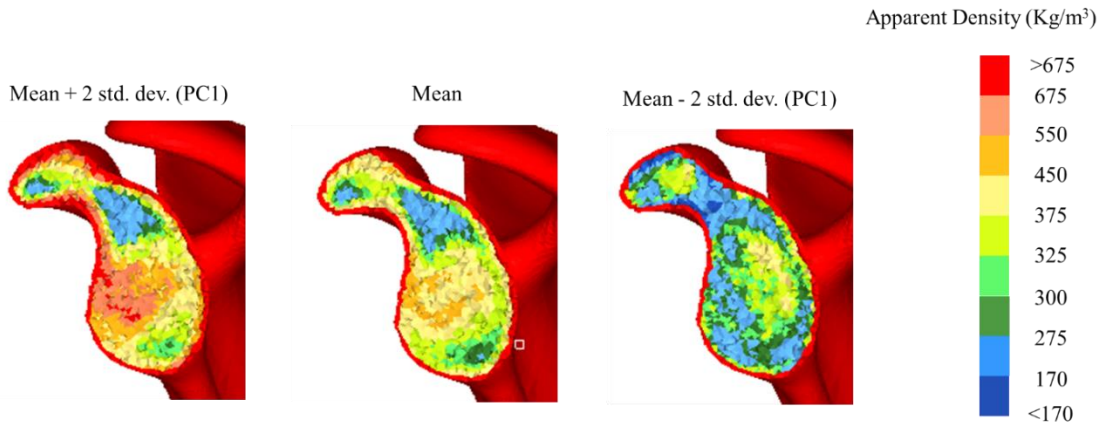

Figure 4.4 Scapula SIM. First mode of variation is shown at mean ± 2 st. dev.. Material properties are overlayed to the mean geometry.

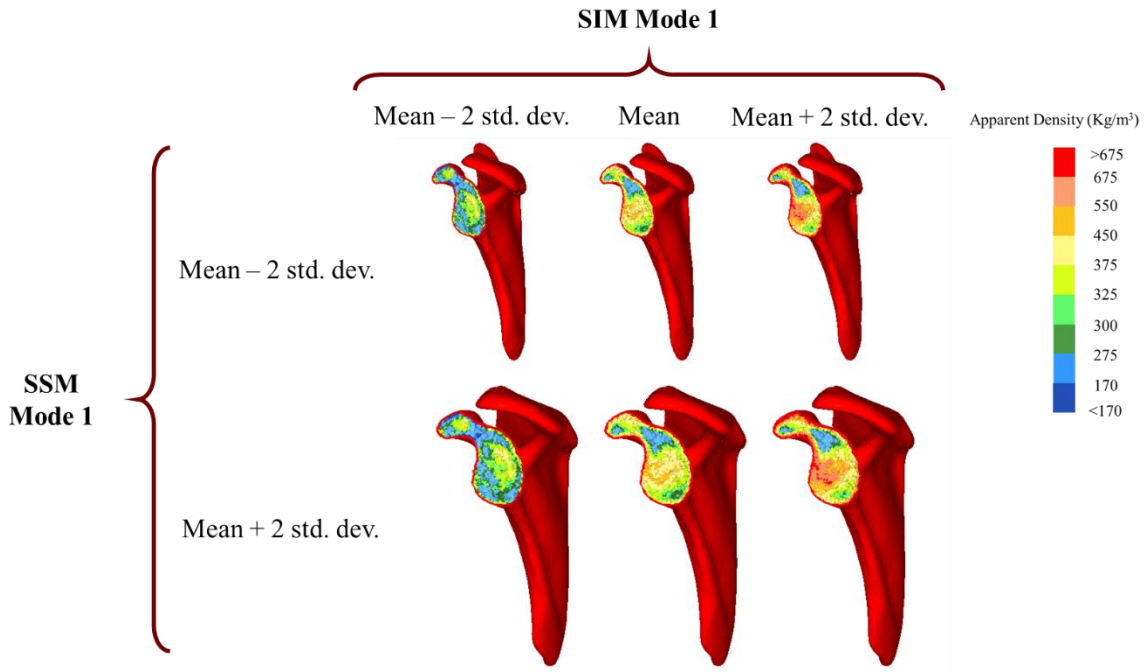

Figure 4.5 Overlay of bony material property genderated from the SIM (mean ± 2 st. dev. of Mode 1) on geometries generated from the SSM (mean ± 2 st. dev. of Mode 1).

CHAPTER 5. CONCLUSIONS AND RECOMMENDATIONS

The studies presented in this thesis advance the current understanding of morphological and material properties variation in the glenohumeral joint bones across the population. The statistical shape and intensity models quantified and described anatomical variation in the proximal humerus and the scapula for training sets of healthy subjects and cadavers, without any bony deformity. The training sets consisted of both genders and three different ethnicities, thus they represented proper samples of the entire population.

The statistical shape and intensity models presented in this work can be used as a supportive infrastructure for population-based studies. Specifically, since implants are still designed and manufactured in discrete sizes for the entire population, statistical models can provide insights on whether to differentiate implant designs and sizing based on gender and ethnicity and on how to optimally discretize sizes so that each one fits the maximum number of patients. The statistical models presented in this thesis suggest that no specific gender effect exists for either the scapula or the humerus, apart from a scaling effect between males and females. However, Asians subjects showed statistically significant higher humeral cortical thickness with respect to the Caucasian subjects. This finding suggests that TSA humeral stems as well as screws and plates for trauma surgery should be designed to accommodate the variation observed, including the differences noted with ethnicity. Additionally, SSM can be used to quickly derive anatomical relationships. Having the bone geometries aligned and registered to the same template dramatically

reduces the time and manual work required to compute anatomical measurements. Access to clinically relevant anatomical measurements for the entire population and for customized sub-populations, e.g. Asians females or Caucasian males, is useful from an implant design and sizing perspective. SSM also finds application in the field of computer-assisted surgery. The predictive capabilities of statistical shape modeling can be used to reconstruct the geometry of the bone from clinical x-rays/fluoroscopy and/or probed points that the surgeon can register during surgery. This is particularly beneficial for the TSA surgery, where exposure of the glenoid is limited. Being able to reconstruct and visualize the entire shape of the glenoid would be helpful for the surgeon for an optimal placement of the glenoid component's, e.g. how many screws to use and their best orientation.

Both studies present limitations. Although the training sets were larger in size than previous studies (>50 for the scapula and >80 for the humerus), the distribution of ethnicity is not representative of the world's population. For example, only two African American subjects were present and this limited the possibility of parsing the data by subgroups. In the scapula model, assessing the thickness of the cortical shell is quite difficult, due to potential artifacts associated with discretization in the geometry and imaging. In our approach, the cortical bone thickness was assumed homogeneous throughout the population, but we could potentially improve future finite-element analysis by differentiating the cortical thickness in each subject.

A potential development of this work would be a material mapping of the humeral bone, which could provide insight for design of humeral screws, plates, implants and surgical instruments. The models developed in this work are finite-element ready. This

feature provides several opportunities for further research, such as finite-element analysis of the glenoid cancellous bone and screw interaction. In addition, having access to a statistical description of the population can help in selecting or generating subjects that capture the variability across the population. Thus, finite-element simulations can be performed only on selected subjects instead of on the entire population, reducing computational costs.

In closing, this work developed a comprehensive approach to characterize the anatomy of the bones of the shoulder. By including a larger training set with diversity in gender and ethnicity, and representation of the internal cancellous bone (humerus) and material property map (scapula), this work advances the current state of the art. The findings quantify the variation present and can help improve implant design and sizing, and influence surgical practice, specifically around guidelines for implant alignment, with the goal of improving TSA outcomes.

BIBLIOGRAPHY

Anglin, C., Tilehurst, P., Wyss, U.P. and Pichora, D.R., 1999. Glenoid cancellous bone strength and modulus. *Journal of biomechanics*, *32*(10), pp.1091-1097.

Anglin, C., Tolhurst, P., Wyss, U.P. and Pichora, D.R., 1999. Glenoid cancellous bone strength and modulus. Journal of biomechanics, 32(10), pp.1091-1097.

Ballmer, F.T., Sidles, J.A., Lippitt, S.B. and Matsen, F.A., 1993. Humeral head prosthetic arthroplasty: surgically relevant geometric considerations. *Journal of Shoulder and Elbow Surgery*, *2*(6), pp.296-304.

Besl, P.J. and McKay, N.D., 1992. A method for registration of 3-D shapes. *IEEE Transactions on pattern analysis and machine intelligence*, 14(2), pp.239-256.

Bohsali, K.I., Wirth, M.A. and Rockwood, C.A., 2006. Complications of total shoulder arthroplasty. *J Bone Joint Surg Am*, *88*(10), pp.2279-2292.

Boileau, P. and Walch, G., 1997. The three-dimensional geometry of the proximal humerus. *J Bone Joint Surg Br*, *79*(5), pp.857-865.

Bredbenner, T.L., Eliason, T.D., Potter, R.S., Mason, R.L., Havill, L.M. and Nicolella, D.P., 2010. Statistical shape modeling describes variation in tibia and femur surface geometry between Control and Incidence groups from the osteoarthritis initiative database. *Journal of biomechanics*, 43(9), pp.1780-1786.

Bryan, R., Mohan, P.S., Hopkins, A., Galloway, F., Taylor, M. and Nair, P.B., 2010. Statistical modelling of the whole human femur incorporating geometric and material properties. *Medical engineering & physics*, *32*(1), pp.57-65.

Campbell, J.Q. and Petrella, A.J., 2016. Automated finite element modeling of the lumbar spine: Using a statistical shape model to generate a virtual population of models. *Journal of biomechanics*, *49*(13), pp.2593-2599.

Campoli, G., Baka, N., Kaptein, B.L., Valstar, E.R., Zachow, S., Weinans, H. and Zadpoor, A.A., 2014. Relationship between the shape and density distribution of the femur and its natural frequencies of vibration. *Journal of biomechanics*, 47(13), pp.3334-3343.

Churchill, R. Sean, John J. Brems, and Helmuth Kotschi. "Glenoid size, inclination, and version: an anatomic study." *Journal of Shoulder and Elbow Surgery* 10.4 (2001): 327-332.

Cootes, T.F. and Taylor, C.J., 2001, July. Statistical models of appearance for medical image analysis and computer vision. In *Proc. SPIE medical imaging* (Vol. 4322, No. 236-248, p. 5).

Darling, A.L., Hakim, O.A., Horton, K., Gibbs, M.A., Cui, L., Berry, J.L., Lanham-New, S.A. and Hart, K.H., 2013. Adaptations in tibial cortical thickness and total volumetric bone density in postmenopausal South Asian women with small bone size. *Bone*, *55*(1), pp.36-43.

Day, J.S., Lau, E., Ong, K.L., Williams, G.R., Ramsey, M.L. and Kurtz, S.M., 2010. Prevalence and projections of total shoulder and elbow arthroplasty in the United States to 2015. *Journal of Shoulder and Elbow Surgery*, *19*(8), pp.1115-1120.

DeLude, J.A., Bicknell, R.T., MacKenzie, G.A., Ferreira, L.M., Dunning, C.E., King, G.J., Johnson, J.A. and Drosdowech, D.S., 2007. An anthropometric study of the bilateral anatomy of the humerus. *Journal of shoulder and elbow surgery*, *16*(4), pp.477-483.

Ding, C. and He, X., 2004, July. K-means clustering via principal component analysis. In *Proceedings of the twenty-first international conference on Machine learning* (p. 29). ACM.

Doerfler, H.M., Huempfner-Hierl, H., Kruber, D., Schulze, P. and Hierl, T., 2017. Template-Based Orbital Wall Fracture Treatment Using Statistical Shape Analysis. *Journal of Oral and Maxillofacial Surgery*, 75(7), pp.1475e1-1475e8.

Drew, A., Cates, J. Morris, M.S.C. and Bachus, K.N. 2014. Statistical shape modeling of the humerus for rapid endoprosthetic stem design iteration. Poster 0963 at *Orthopaedic Research Society 2014 Annual Meeting*, March 15-18 2014, New Orleans, Lousiana.

Fitzpatrick, C.K., Baldwin, M.A., Laz, P.J., FitzPatrick, D.P., Lerner, A.L. and Rullkoetter, P.J., 2011. Development of a statistical shape model of the patellofemoral joint for investigating relationships between shape and function. *Journal of biomechanics*, *44*(13), pp.2446-2452.

Fitzpatrick, C.K., FitzPatrick, D.P. and Auger, D.D., 2008. Size and shape of the resection surface geometry of the osteoarthritic knee in relation to total knee replacement

design. *Proceedings of the Institution of Mechanical Engineers, Part H: Journal of Engineering in Medicine, 222*(6), pp.923-932.

Frankle, Mark A., et al. "Glenoid morphology in reverse shoulder arthroplasty: classification and surgical implications." *Journal of shoulder and elbow surgery* 18.6 (2009): 874-885.

Frich, L. H., 1994. Glenoid Knoglestyrke og knoglestruktur. Doctoral thesis, University of Aarhus, Aarhus, Denmark.

Frich, L.H., Jensen, N.C., Odgaard, A., Pedersen, C.M., Søjbjerg, J.O. and Dalstra, M., 1997. Bone strength and material properties of the glenoid. *Journal of Shoulder and Elbow Surgery*, 6(2), pp.97-104.

Frich, L.H., Odgaard, A. and Dalstra, M., 1998. Glenoid bone architecture. J*ournal of Shoulder and Elbow Surgery*, 7(4), pp.356-361.

Fulin, P., Kysilko, M., Pokorny, D., Padr, R., Kasprikova, N., Landor, I. and Sosna, A., 2017. Study of the variability of scapular inclination and the glenoid version-considerations for preoperative planning: clinical-radiological study. *BMC Musculoskeletal Disorders*, *18*(1), p.16.

Galloway, F., Kahnt, M., Ramm, H., Worsley, P., Zachow, S., Nair, P. and Taylor, M., 2013. A large scale finite element study of a cementless osseointegrated tibial tray. *Journal of biomechanics*, 46(11), pp.1900-1906.

Gebhart, J.J., Miniaci, A. and Fening, S.D., 2013. Predictive anthropometric measurements for humeral head curvature. *Journal of Shoulder and Elbow Surgery*, *22*(6), pp.842-847.

Ghafurian, S., Galdi, B., Bastian, S., Tan, V. and Li, K., 2015. Computerized 3D morphological analysis of glenoid orientation. *Journal of Orthopaedic Research*, 34(4), pp. 692-698.

Godenèche, A., Boileau, P., Favard, L., Le Huec, J.C., Lévigne, C., Nové-Josserand, L., Walch, G. and Edwards, T.B., 2002. Prosthetic replacement in the treatment of osteoarthritis of the shoulder: early results of 268 cases. *Journal of shoulder and elbow surgery*, *11*(1), pp.11-18.

Hasan, S.S., Leith, J.M., Campbell, B., Kapil, R., Smith, K.L. and Matsen, F.A., 2002. Characteristics of unsatisfactory shoulder arthroplasties. *Journal of shoulder and elbow surgery*, 11(5), pp.431-441.

Hertel, R., Knothe, U. and Ballmer, F.T., 2002. Geometry of the proximal humerus and implications for prosthetic design. *Journal of shoulder and elbow surgery*, *11*(4), pp.331-338.

Horn, J.L., 1965. A rationale and test for the number of factors in factor analysis. *Psychometrika*, 30(2), pp.179-185.

Hovinga, K.R. and Lerner, A.L., 2009. Anatomic variations between Japanese and Caucasian populations in the healthy young adult knee joint. *Journal of Orthopaedic Research*, 27(9), pp.1191-1196.

Humphrey, C.S., Sears, B.W. and Curtin, M.J., 2016. An anthropometric analysis to derive formulae for calculating the dimensions of anatomically shaped humeral heads. *Journal of Shoulder and Elbow Surgery*, *25*(9), pp.1532-1541.

Jolliffe, I., 2002. *Principal component analysis*. John Wiley & Sons, Ltd.

Kalouche, I., Crépin, J., Abdelmoumen, S., Mitton, D., Guillot, G. and Gagey, O., 2010. Mechanical properties of glenoid cancellous bone. *Clinical Biomechanics*, *25*(4), pp.292-298.

Kamer, L., Noser, H., Popp, A.W., Lenz, M. and Blauth, M., 2016. Computational anatomy of the proximal humerus: An ex vivo high-resolution peripheral quantitative computed tomography study. *Journal of Orthopaedic Translation*, *4*, pp.46-56.

Keyak, J.H., Rossi, S.A., Jones, K.A., Les, C.M. and Skinner, H.B., 2001. Prediction of fracture location in the proximal femur using finite element models. *Medical engineering & physics*, 23(9), pp.657-664.

Lamecker, H., Seebaß, M., Hege, H.C. and Deuflhard, P., 2004, February. A 3 D statistical shape model of the pelvic bone for segmentation. In *Proceedings of SPIE* (Vol. 5370, pp. 1341-1351).

Laz, P.J. and Browne, M., 2010. A review of probabilistic analysis in orthopaedic biomechanics. *Proceedings of the Institution of Mechanical Engineers, Part H: Journal of Engineering in Medicine*, 224(8), pp.927-943

Lehtinen, J.T., Tingart, M.J., Apreleva, M. and Warner, J.J., 2004. Total, trabecular, and cortical bone mineral density in different regions of the glenoid. *Journal of shoulder and elbow surgery*, 13(3), pp.344-348.

Mahfouz, M., Fatah, E.E.A., Bowers, L.S. and Scuderi, G., 2012. Three-dimensional morphology of the knee reveals ethnic differences. *Clinical Orthopaedics and Related Research*, *470*(1), pp.172-185.

Mansat, P., Barea, C., Hobatho, M.C., Darmana, R. and Mansat, M., 1998. Anatomic variation of the mechanical properties of the glenoid. *Journal of Shoulder and Elbow Surgery*, *7*(2), pp.109-115.

Mathews, S., Burkhard, M., Serrano, N., Link, K., Häusler, M., Frater, N., Franke, I., Bischofberger, H., Buck, F.M., Gascho, D. and Thali, M., 2017. Glenoid morphology in light of anatomical and reverse total shoulder arthroplasty: a dissection-and 3D-CT-based study in male and female body donors. *BMC Musculoskeletal Disorders*, *18*(1), p.9.

Matsen, F.A., Clinton, J., Lynch, J., Bertelsen, A. and Richardson, M.L., 2008. Glenoid component failure in total shoulder arthroplasty. J Bone Joint Surg Am, 90(4), pp.885-896.

Matsumura, Noboru, et al. "Morphologic features of humeral head and glenoid version in the normal glenohumeral joint." *Journal of shoulder and elbow surgery* 23.11 (2014): 1724-1730.

Mayya, M., Poltaretskyi, S., Hamitouche, C. and Chaoui, J., 2013, April. Scapula Statistical Shape Model construction based on watershed segmentation and elastic registration.

In Biomedical Imaging (ISBI), 2013 IEEE 10th International Symposium on (pp. 101-104). IEEE.

McPherson, E.J., Friedman, R.J., An, Y.H., Chokesi, R. and Dooley, R.L., 1997. Anthropometric study of normal glenohumeral relationships. *Journal of Shoulder and Elbow Surgery*, 6(2), pp.105-112.

Merrill, Andrea, Kara Guzman, and Suzanne L. Miller. "Gender differences in glenoid anatomy: an anatomic study." *Surgical and radiologic anatomy* 31.3 (2009): 183-189.

Mimar, R., Limb, D. and Hall, R.M., 2008. Evaluation of the mechanical and architectural properties of glenoid bone. *Journal of Shoulder and Elbow Surgery*, 17(2), pp.336-341.

Morgan, E.F., Bayraktar, H.H. and Keaveny, T.M., 2003. Trabecular bone modulus–density relationships depend on anatomic site. *Journal of biomechanics*, 36(7), pp.897-904.

Mutsvangwa, T., Burdin, V., Schwartz, C. and Roux, C., 2015. An automated statistical shape model developmental pipeline: application to the human scapula and humerus. *IEEE Transactions on Biomedical Engineering*, *62*(4), pp.1098-1107.

Myronenko, A. and Song, X., 2010. Point set registration: Coherent point drift. IEEE transactions on pattern analysis and machine intelligence, 32(12), pp.2262-2275.

Nelson, D.A., Pettifor, J.M., Barondess, D.A., Cody, D.D., Uusi-Rasi, K. and Beck, T.J., 2004. Comparison of Cross-Sectional Geometry of the Proximal Femur in White and Black

Women from Detroit and Johannesburg. *Journal of Bone and Mineral Research*, *19*(4), pp.560-565.

Nicolella, D.P. and Bredbenner, T.L., 2012. Development of a parametric finite element model of the proximal femur using statistical shape and density modelling. Computer methods in biomechanics and biomedical engineering, 15(2), pp.101-110.

Pearl, M.L. and Kurutz, S., 1999. Geometric analysis of commonly used prosthetic systems for proximal humeral replacement. *J Bone Joint Surg Am*, *81*(5), pp.660-71.

Pearl, M.L. and Volk, A.G., 1996. Coronal plane geometry of the proximal humerus relevant to prosthetic arthroplasty. *Journal of Shoulder and Elbow Surgery*, *5*(4), pp.320-326.

Pearl, M.L., Kurutz, S. and Postachini, R., 2009. Geometric variables in anatomic replacement of the proximal humerus: how much prosthetic geometry is necessary? *Journal of Shoulder and Elbow Surgery*, *18*(3), pp.366-370.

Querol, L., Büchler, P., Rueckert, D., Nolte, L. and Ballester, M., 2006. Statistical finite element model for bone shape and biomechanical properties. *Medical Image Computing and Computer-Assisted Intervention–MICCAI 2006*, pp.405-411.

Roberson, T.A., Bentley, J.C., Griscom, J.T., Kissenberth, M.J., Tolan, S.J., Hawkins, R.J. and Tokish, J.M., 2017. Outcomes of total shoulder arthroplasty in patients younger than 65 years: a systematic review. *Journal of Shoulder and Elbow Surgery*.

Robertson, D.D., Yuan, J., Bigliani, L.U., Flatow, E.L. and Yamaguchi, K., 2000. Three-dimensional analysis of the proximal part of the humerus: relevance to arthroplasty. *J Bone Joint Surg Am*, *82*(11), pp.1594-1594.

Sanchez-Sotelo, J., 2006. Proximal humerus fractures. *Clinical Anatomy*, 19(7), pp.588-598.

Schileo, E., Dall'Ara, E., Taddei, F., Malandrino, A., Schotkamp, T., Baleani, M. and Viceconti, M., 2008. An accurate estimation of bone density improves the accuracy of subject-specific finite element models. *Journal of biomechanics*, *41*(11), pp.2483-2491

Schumann, S., Bieck, R., Bader, R., Heverhagen, J., Nolte, L.P. and Zheng, G., 2016. Radiographic reconstruction of lower-extremity bone fragments: a first trial. *International journal of computer assisted radiology and surgery*, 11(12), pp.2241-2251.

Smoger, L.M., Fitzpatrick, C.K., Clary, C.W., Cyr, A.J., Maletsky, L.P., Rullkoetter, P.J. and Laz, P.J., 2015. Statistical modeling to characterize relationships between knee anatomy and kinematics. *Journal of Orthopaedic Research*, 33(11), pp.1620-1630.

Vrancken, A.C.T., Crijns, S.P.M., Ploegmakers, M.J.M., O'kane, C., Tienen, T.G., Janssen, D., Buma, P. and Verdonschot, N., 2014. 3D geometry analysis of the medial meniscus–a statistical shape modeling approach. *Journal of anatomy*, 225(4), pp.395-402.

Waarsing, J.H., Rozendaal, R.M., Verhaar, J.A.N., Bierma-Zeinstra, S.M.A. and Weinans, H., 2010. A statistical model of shape and density of the proximal femur in relation to radiological and clinical OA of the hip. *Osteoarthritis and cartilage*, 18(6), pp.787-794.

Werner, Birgit S., et al. "The influence of three-dimensional planning on decision-making in total shoulder arthroplasty." *Journal of Shoulder and Elbow Surgery* (2017).

Wu, G., Van der Helm, F.C., Veeger, H.D., Makhsous, M., Van Roy, P., Anglin, C., Nagels, J., Karduna, A.R., McQuade, K., Wang, X. and Werner, F.W., 2005. ISB recommendation on definitions of joint coordinate systems of various joints for the reporting of human joint motion—Part II: shoulder, elbow, wrist and hand. *Journal of biomechanics*, *38*(5), pp.981-992.

Yang, Y.M., Rueckert, D. and Bull, A.M., 2008. Predicting the shapes of bones at a joint: application to the shoulder. *Computer Methods in Biomechanics and Biomedical Engineering*, *11*(1), pp.19-30.

APPENDIX A. ANATOMICAL MEASUREMENTS AND ANATOMICAL COORDINATE SYSTEMS

The template anatomical coordinate systems were defined similarly to Wu et al., 2005. For the humerus, the origin was placed in the glenohumeral rotational center, estimated as the center of the best-fitting sphere for the humeral head; the mediolateral axis was defined by the direction of the segment connecting the two epicondyles, pointing medially; the anterior-posterior axis was defined as the perpendicular to the plane of the glenohumeral rotational center and the epicondyles, pointing anteriorly; the superior-inferior axis was defined consequently to form a right-hand coordinate system (Figure A.1). For the scapula, the origin was placed in the center of the glenoid; the mediolateral axis was defined by the direction of the segment connecting the angulus acromialis and the trigonum scapulae, pointing laterally; the anterior-posterior axis was defined as the perpendicular to the plane formed by the angulus inferior, angulus acromialis and the trigonum scapulae, pointing anteriorly; the superior-inferior axis was defined consequently to form a right-hand coordinate system (Figure A.1).

Anatomical landmarks were manually placed on the template geometries (Figure A.2) and then automatically selected on each registered subject, based on node numbers. They were used to automatically compute anatomical measurements on each registered subject and to build the anatomical coordinate systems.

- **Humerus**

1. Greater tuberosity (GT)
2. Most anterior point of the anatomic neck (MA)
3. Most posterior point of the anatomic neck (MP)
4. Most lateral point of the anatomic neck (ML)
5. Most medial point of the anatomic neck (MM)
6. Superior apex of the head (SA)

- **Scapula**

1. Glenoid center (GC)
2. Most inferior point of the glenoid rim (INF)
3. Most superior point of the glenoid rim (SUP)
4. Most anterior point of the glenoid rim (ANT)
5. Most posterior point of the glenoid rim (POST)
6. Angulus acromialis (AA)
7. Angulus inferior (AI)
8. Trigonum scapulae (TS)

Humerus and scapula anatomical measurements were computed as follows.

- **Humerus**

1. Head radius

The head radius was computed as the radius of the sphere that best fits the humeral head (Figure A.3), i.e. the epiphyseal sphere (Boileau and Walch, 1997). The nodes used to find the best-fitting sphere are selected manually on the cortical shell of the template and then used for all the subjects in the register.

2. *Canal diameter*

   The canal diameter was computed as the diameter of the cylinder that best fits the most inferior half of the cancellous shaft (Figure A.3), i.e. the metaphyseal cylinder (Boileau and Walch, 1997). The axis of this cylinder is the canal axis (orthopaedic axis). This method gives an estimate that does not consider how the canal diameter may vary along the shaft. If it is of interest to compute the diameter at specific sections of the shaft, this can be measured as the minimum distance between the most anterior and the most posterior point and the most medial and the most lateral point, or as the diameter of the best-fitting circle.

3. *Head sphericity*

   Head sphericity was computed as the ratio between the radii of the best-fitting circles in the X (mediolateral) - Z (superior-inferior) plane and Y (anterior-posterior) - Z (superior-inferior) plane (Figure A.4). X-Z is the frontal plane; Y-Z is the sagittal plane. The points used to find the best-fitting circles come from the projections of the points used to find the best-fitting sphere on the fontal and sagittal plane; to make the code more robust, only the points above the origin are selected.

4. *Anatomical neck angle*

   The anatomic neck angle was computed as the angle that the vector connecting the most medial point of the anatomic neck and the most lateral point of the anatomic neck forms with the Z-axis (Figure A.5).

5. *Greater tuberosity offset (or critical distance)*

As defined in (Hertel et al., 2002), the greater tuberosity offset (or critical distance) is the distance between the most medial point of the anatomical neck and the canal axis in the X (mediolateral) - Z (superior-inferior) plane (Figure A.5).

6. *Articular surface thickness*

   As defined in (Boileau and Walch, 1997), the articular surface thickness is the distance between the articular margin plane and the superior apex of the head, in the X (mediolateral) - Z (superior-inferior) plane (Figure A.5).

7. *Inclination angle of the head*

   As defined in (Boileau and Walch, 1997), the inclination angle of the head is the angle between the canal axis and the perpendicular to the articular margin plane, in the X (mediolateral) - Z (superior-inferior) plane (Figure A.5).

8. *Medial offset*

   As defined in (Boileau and Walch, 1997), the medial offset is the distance between the head center (i.e. the center of the best-fitting sphere) and the canal axis in the X (mediolateral) - Z (superior-inferior) plane (Figure A.6).

9. *Anterior-posterior offset*

   As defined in (Boileau and Walch, 1997), the anterior-posterior offset is the distance between the head center (i.e. the center of the best-fitting sphere) and the canal axis in the Y (anterior-posterior) - Z (superior-inferior) plane (Figure A.6).

10. *Cortical thickness*

The cortical thickness was computed as the distance between the cortical and the cancellous profile, at a specific section of the shaft, and at various angles (Figure A.7). The distance was calculated both along the radial direction and along a direction normal to the cortical profile. An alternative, quicker method could be to calculate the difference between the diameter of the best-fitting cylinder in the cancellous bone and the best-fitting cylinder in the cortical bone.

Only the proximal portion of the humerus was included in the SSM. The humerus shaft was resected at the intersection with a sphere whose center was placed coincident with the head center and whose radius was proportional to the head radius (5.6 times). Given that the SSM was developed only on the proximal portion of the humerus, it was not possible to calculate the retroversion angle, since it is based on the transepycondilar axis.

- **Scapula**

1. *Anterior-posterior glenoid diameter*

   The anterior-posterior glenoid diameter was computed as the diameter of the best-fitting circle of the inferior portion of the glenoid (Figure A.8). The points used to find the best-fitting circle were selected manually on the template's glenoid and then used for all the subjects in the register. To find the best-fitting circle, these points were projected on the plane of the glenoid face.

2. *Superior-inferior glenoid diameter*

The superior-inferior glenoid diameter was computed as the longest dimension of the best-fitting ellipse in the glenoid (Figure A.9). The points used to find the best-fitting ellipse were selected manually on the template's glenoid and then used for all the subjects in the register. To find the best-fitting ellipse, these points were projected on the plane of the glenoid face.

3. *Anterior-posterior glenoid radius of curvature*

   The anterior-posterior radius of curvature, i.e. radius of curvature in the transverse plane, was calculated as the radius of the best-fitting circle on the glenoid face (Figure A.10).

4. *Superior-inferior glenoid radius of curvature*

   The superior-inferior radius of curvature, i.e. radius of curvature in the coronal plane, was calculated as the radius of the best-fitting circle on the glenoid face (Figure A.10).

5. *Glenoid circularity*

   Glenoid circularity was calculated as the ratio between the superior-inferior and the anterior-posterior diameters.

6. *Glenoid inclination angle*

   The inclination angle was calculated as the angle that the direction of the superior-inferior diameter forms with the Z-axis. To compute the inclination angle, the scapula was brought in the YZ plane and rotated about the Z-axis until the new X-axis was coincident with the vector describing the anterior-posterior glenoid diameter (Figure A.11).

7. Glenoid retroversion angle

As in (Friedman et al., 1992) and in (Matsumura et al., 2014), the retroversion angle was calculated as the angle between the glenoid line, i.e. line connecting the most anterior and most posterior points of the glenoid rim, and the line perpendicular to the scapular axis, in the X-Y plane. The scapular axis was defined as the line connecting the center of the glenoid, i.e. the center of the best-fitting ellipse, with the trigonum scapulae (Figure A.11).

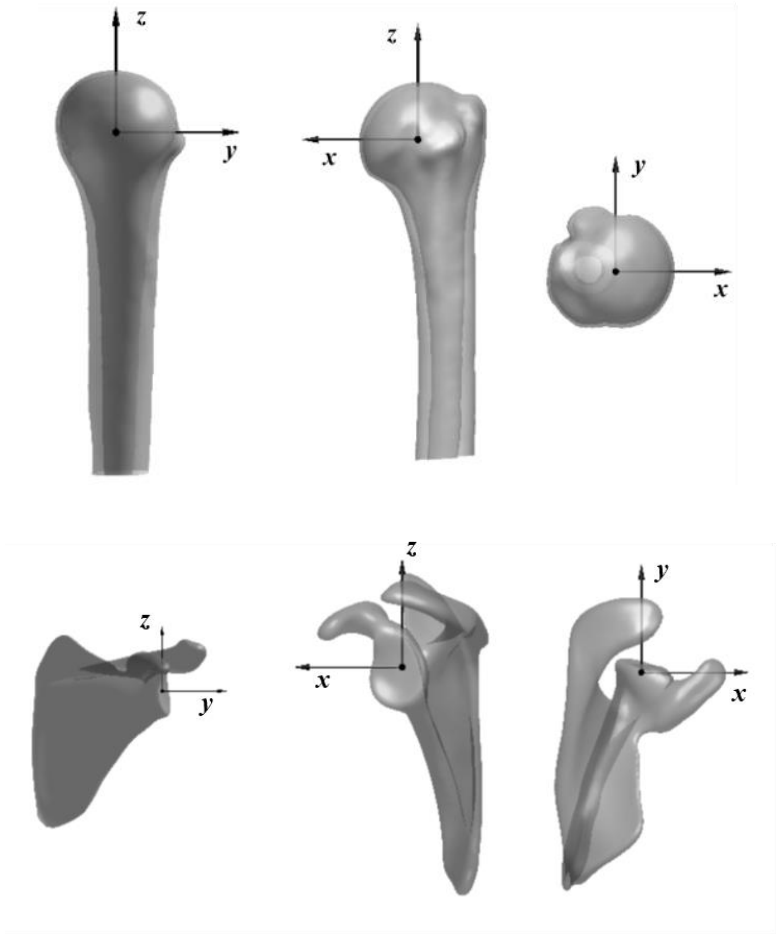

Figure A.1 Humerus (above) and scapula (below) templates anatomical coordinate systems.

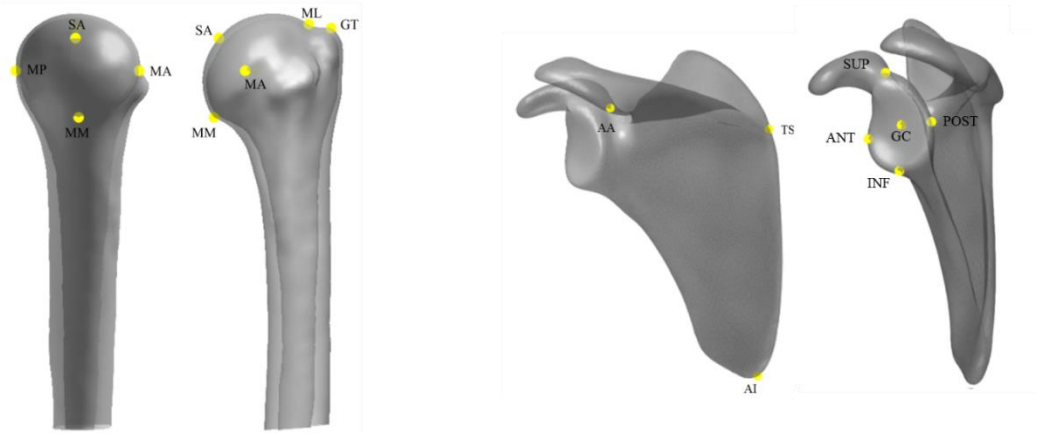

Figure A.2 Humerus (left) and scapula (right) anatomical landmarks.

Figure A.3 Best-fitting cylinder for the metaphyseal cylinder (left) and the best-fitting sphere for the humeral head (right). The cortical nodes used to find the best-fitting geometries are represented as yellow scattered points; the analytical surfaces are represented in shaded yellow.

Figure A.4 Best-fitting circles for the humeral head in the sagittal (left) and frontal (right) plane. The scattered points in yellow are the nodes used to find the best-fitting circles (see Figure A3).

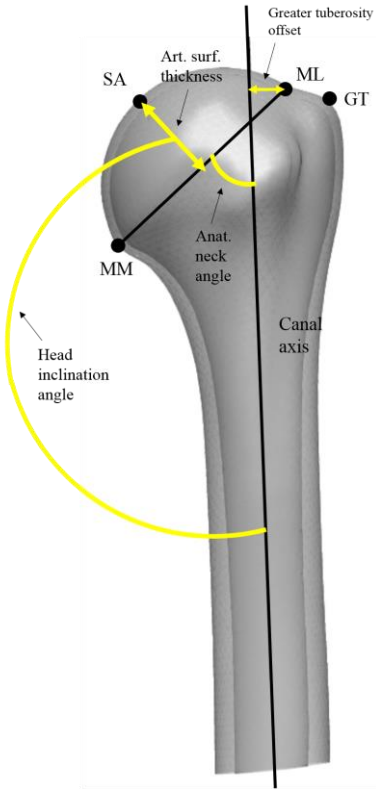

Figure A.5 The humerus is represented in the X-Z plane to show the anatomical neck angle, the greater tuberosity offset or critical distance, the head inclination angle and the articular surface thickness.

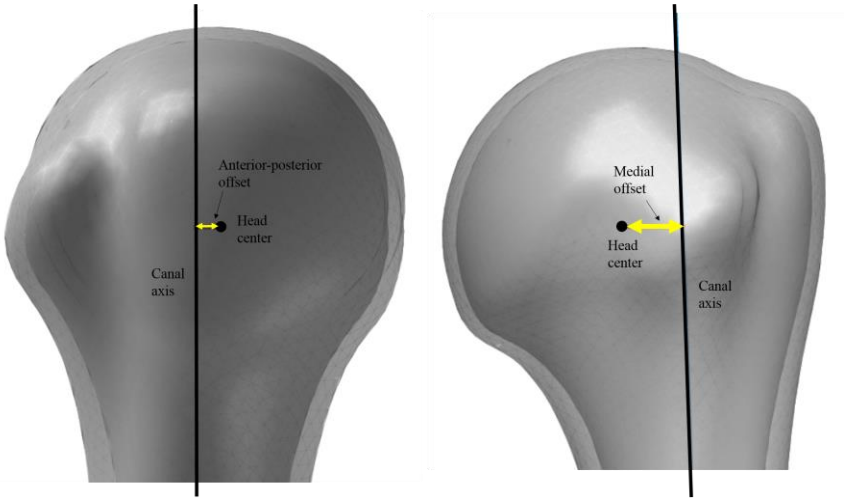

Figure A.6 The humeral head is represented in the Y-Z plane (left) and the X-Z plane (right) to show respectively the anterior-posterior offset and the medial offset.

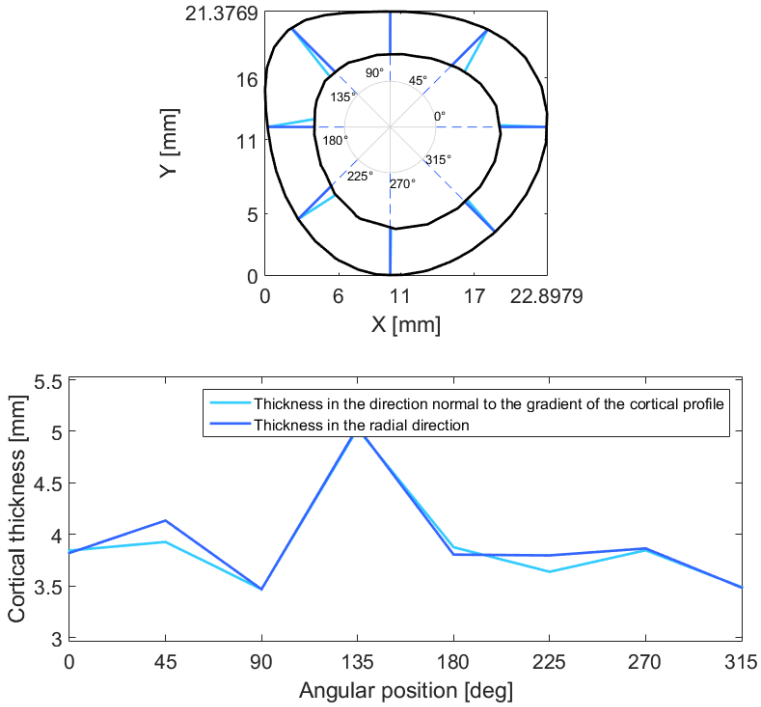

Figure A.7 Cortical thickness was measured as the distance between cortical and cancellous profile at a specific section of the shaft (80 mm below the origin, for the case showed here), at various angles.

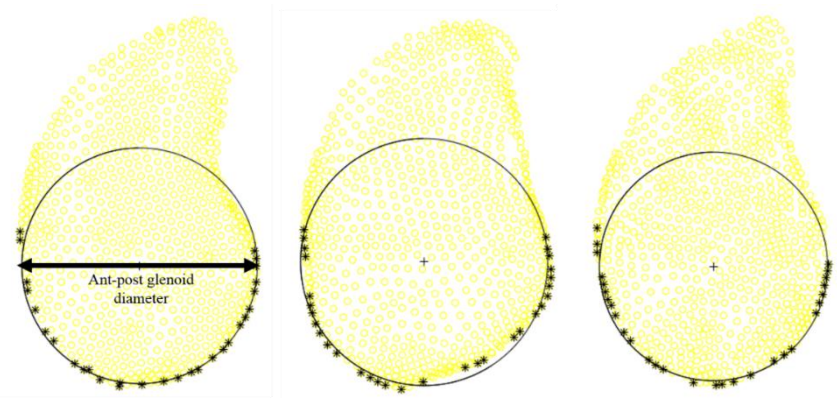

Figure A.8 Best-fitting circles on the inferior glenoid surfaces for three representative subjects. The yellow scattered points are the nodes used to represent the glenoid surface; the black asterisks are the points used to find the best-fitting circles.

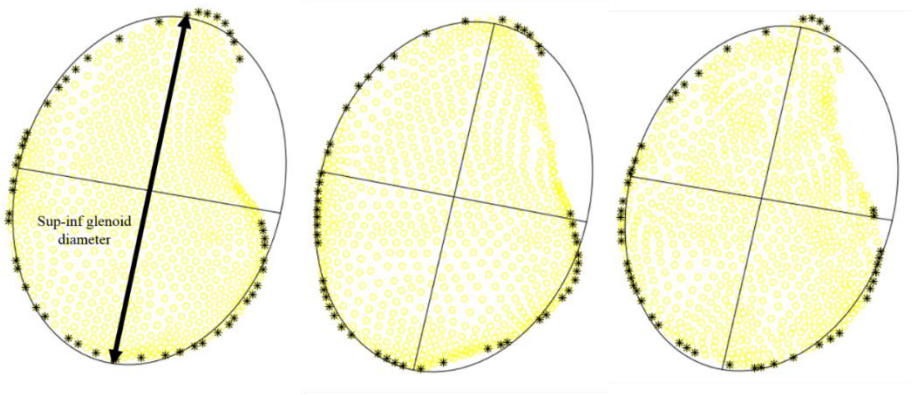

Figure A.9 Best-fitting ellipses on the glenoid surfaces for three representative subjects. The yellow scattered points are the nodes used to represent the glenoid surface; the black asterisks are the points used to find the best-fitting ellipses.

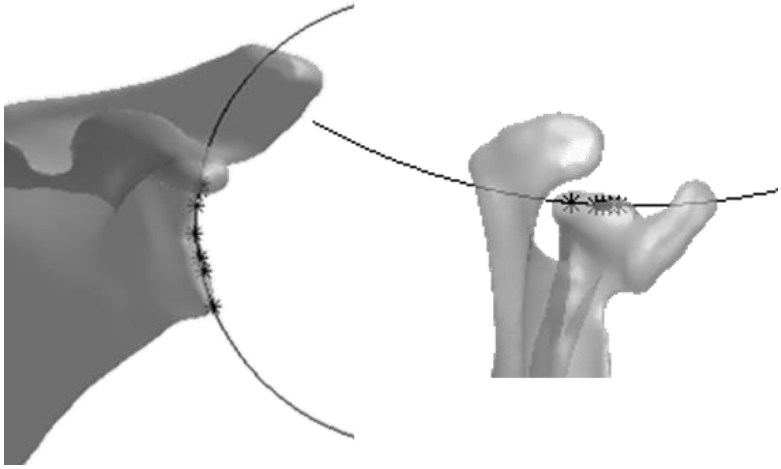

Figure A.10 Best-fitting circles used to find the glenoid radii of curvature in the coronal (left) and transverse (right) planes.

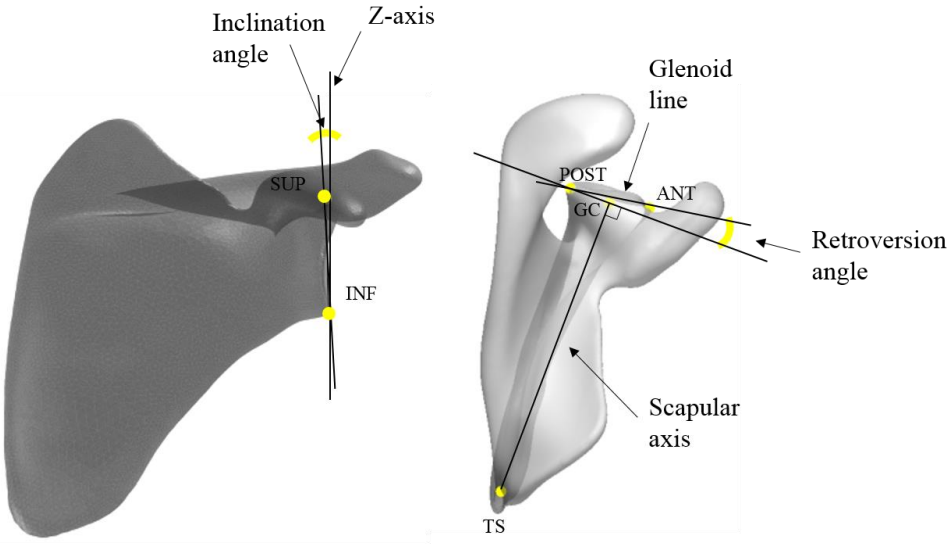

Figure A.11 Inclination angle (left) was defined as the angle that the vector connecting the most inferior (INF) and most superior (SUP) glenoid points forms with the Z-axis. Retroversion angle (right) was defined as the angle between the glenoid line and the line perpendicular to the scapular axis, in the X-Y plane. GC is the center of the glenoid; ANT and POST are the most anterior and most posterior points of the glenoid rim; TS is the trigonum scapulae.

APPENDIX B. MATERIAL PROPERTY ASSIGNMENT WORKFLOW

The purpose of the following appendix is to provide a more detailed description of the process that was used to assign material properties to the scapula. Each subject was assigned material properties (i.e., apparent density and elastic modulus) from the CT scan. The process was carried out as follows:

1. The subject was meshed with tetrahedral elements (TET) in Simpleware ScanIP. The element size was about 1 mm, finer that the template mesh of the statistical shape model. The reason behind this choice will be clarified in the following steps. The size of the internal elements was set to be consistent with the size of the surface elements. The material properties of the bone were determined by transforming Hounsfield units (HU) to apparent density, assuming a lower bound threshold of 1 $\frac{Kg}{m^3}$. All the CT scans had been performed using consistent machine settings and a CT calibration phantom (QCT Pro, Mindways Software, Inc., Austin TX) had been included to derive the relationship between cancellous bone mineral density (ρ_{QCT}) and greyscale values, i.e. HU. The following calibration equation was then used to assign material properties:

$$\rho_{QCT} = 0.0006782\ HU - 0.009409 \qquad ({}^{gr}/_{cm^3})$$

Bone mineral density was converted into apparent density using the following relationships (Schileo et al., 2008):

$$\rho_{ash} = \frac{\rho_{QCT} + 0.09}{1.14} \qquad (^{gr}/_{cm^3})$$

$$\rho_{app} = \frac{\rho_{ash}}{0.598} \qquad (^{gr}/_{cm^3})$$

2. Because of surface artifact complications, apparent density of all the elements with at least one node on the surface was set based on the maximum HU for that CT scan. Every location within the bone that had a HU that would give a density lower that 1 $\frac{Kg}{m^3}$ was set at 1 $\frac{Kg}{m^3}$. To assign apparent density, HU values were discretized in 100 groups of elements with the same material properties.
3. Apparent density was converted to Young's modulus using the scapula-specific relationships from Gupta et al., 2004:

$$E = 0.001049\rho^2 \qquad \rho \leq 350\ \frac{Kg}{m^3}$$

$$E = 3{\times}10^{-6}\rho^3 \qquad 350\frac{Kg}{m^3} \leq \rho \leq 1800\ \frac{Kg}{m^3}$$

4. Each element of the TET mesh was assigned apparent density and Young's modulus.
5. The TET mesh was exported as well as a face mesh to be used for the registration algorithm, i.e. to find the rigid body transformation matrix to go from CT scan space to the SSM space.
6. The centroid of each TET element was calculated and it was assigned apparent density and Young's modulus of its respective elements. The material properties were assigned to nodes instead of elements to build the SIM.
7. An Iterative Closest Point (ICP) algorithm was used to find the transformation matrix from the CT scan space (i.e. the space where the TET meshes created in ScanIP were)

to the SSM space (i.e. the space in which the registered TET meshes were), using the face mesh exported from ScanIP. This transformation matrix was applied to each TET mesh exported from ScanIP to align it to the registered TET mesh of the same subject, i.e. the SSM mesh.

8. Each node of the registered TET mesh was assigned density and Young's modulus of the closest centroid of the TET elements exported from ScanIP. This was done performing a nearest-neighbor search. For this step to work properly and accurately, it was important that the registered mesh (average edge length: less than 1.5 mm) was coarser than the mesh exported from ScanIP (average edge length: about 1 mm).
9. All the nodes on the surface were assigned cortical bone material properties (i.e. apparent density corresponding to the maximum HU in the CT scan) to correct for possible different values due to the conversion of element properties into nodal properties.

Table B.1 compares the average density of the glenoid cancellous bone measured from *in vitro* tests to the data obtained from our process.

Table B.1 Comparison between density of the glenoid cancellous bone from *in vitro* experiments and from CT scans.

Source	**Cancellous Density ($\frac{Kg}{m^3}$)**
Frich et al., 1997 (subchondral region, 20 specimen) – *in vitro*	340 ± 100 (bare area) 380 ± 110 (sup. and inf. areas)
Mansat et al., 1998 (entire glenoid, 6 specimens) – *in vitro*	282 ± 60
Lehtinen et al., 2004 (entire glenoid, 20 specimens) – CT scan	Range: 395-557
Current study (glenoid cancellous bone, 53 scapulae) – CT scan	377± 102

APPENDIX C. GRAPHICAL USER INTERFACE FOR STATISTICAL SHAPE AND INTENSITY MODELING

Two Graphical User Interfaces (GUI) were developed in Matlab (Mathworks, Natick, MA) as a supporting tool for TSA implant design. The GUIs allow the user to explore anatomical variation in the humerus and the scapula, to export new geometries generated as combination of PC scores, to import and score new subjects and to plot anatomical measurements for the populations. The GUIs also allow the user to import TSA implants (humeral stem and glenoid component) and to virtually implant them into the bone. Figure C.12 and Figure C.13 shows screenshots of the GUIs.

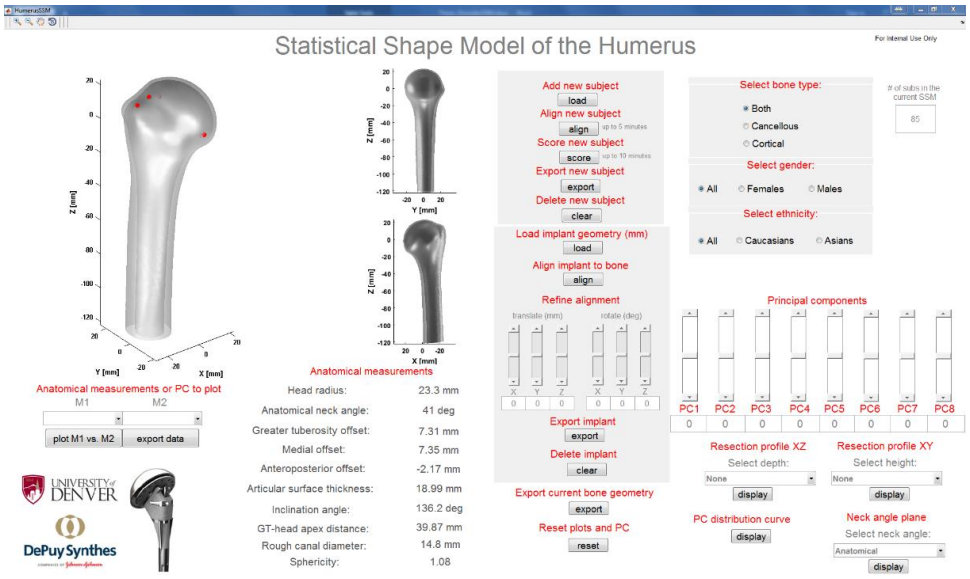

Figure C.12 GUI for the Humerus SSM.

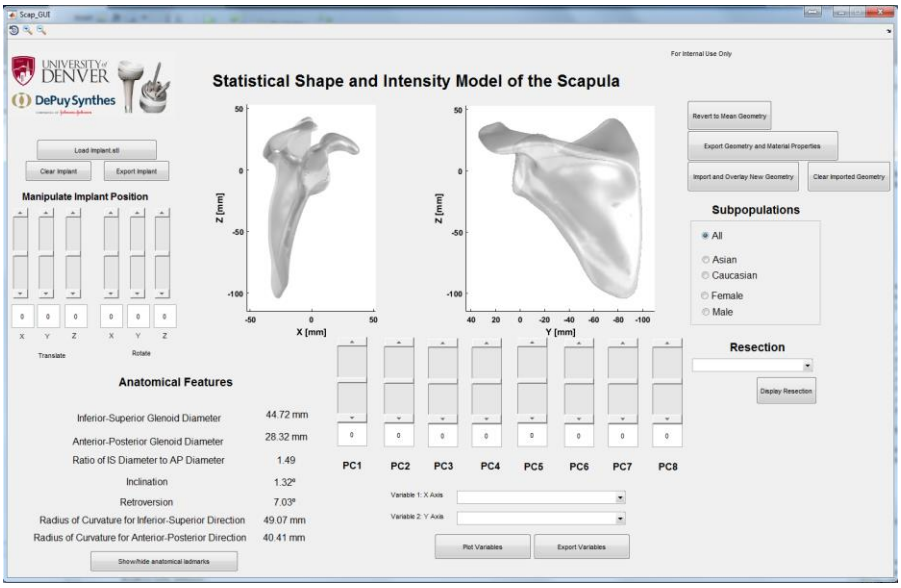

Figure C.13 GUI for the Scapula SSM and SIM.

APPENDIX D. RELATED PUBLICATIONS

I. Sintini, P. Sade, W.S. Burton, J. Chavarria, P.J. Laz (2107). "Statistical shape modeling to quantify variation in proximal humeral anatomy," *63rd Annual Meeting of the Orthopaedic Research Society,* San Diego, CA, 1155, *accepted for poster presentation.*

W.S. Burton, I. Sintini, J. Chavarria, J. Brownhill, P.J. Laz (2017). "Assessment of glenoid anatomy and bone quality using a statistical shape and intensity model," *63rd Annual Meeting of the Orthopaedic Research Society,* San Diego, CA, 0273, *accepted for podium presentation.*

I. Sintini, W.S. Burton, J. Brownhill, P.J. Laz (2107). "Assessing glenohumeral joint conformity with a statistical shape model.," *41st Annual Meeting of the American Society of Biomechanics,* Boulder, CO, 573, *accepted for poster presentation.*